A sub-fossil coral Sr/Ca record documents northward shifts of the Tropical Convergence Zone in the eastern Indian Ocean

Miriam Pfeiffer[1], Hideko Takayanagi[2,3], Lars Reuning[1,] Takaaki K. Watanabe[1,43], Saori Ito[1,3], Dieter Garbe- Schönberg[1], Tsuyoshi Watanabe[43,54,65], Chung-Che Wu[76], Chuan-Chou Shen[87,98], Jens Zinke[109], Geert-Jan A. Brummer[110], Sri Yudawati Cahyarini[121]

[1]Institute of Geosciences, Kiel University, Kiel, 24118, Germany
[2]Institute of Geology and Paleontology, Graduate School of Science, Tohoku University, Aramaki-Aza-Aoba 6-3, Sendai 980-8578, Japan
[3]Advanced Institute for Marine Ecosystem Change (WPI-AIMEC), Tohoku University, Sendai, Japan
[43]KIKAI Institute for Coral Reef Sciences, Kikai Town, Kagoshima 891-6151, Japan.
[54]Department of Natural History Sciences, Faculty of Science, Hokkaido University, Sapporo, 060-0810, Japan
[65]Research Institute for Humanity and Nature (RIHN), Kyoto 603-8047, Japan
[76]College of Marine Sciences and Engineering, Nanjing Normal University, Nanjing, 210023, China
[87]High-Precision Mass Spectrometry and Environment Change Laboratory (HISPEC), Department of Geosciences, National Taiwan University, Taipei, 10617, Taiwan ROC
[98]Research Center for Future Earth, National Taiwan University, Taipei, 10617, Taiwan ROC
[109]School of Geography, Geology and the Environment, University of Leicester, Leicester, LE1 7RH, UK
[110]Department of Ocean Systems, Royal Netherlands Institute for Sea Research (NIOZ), and Utrecht University, 1790 AB Den Burg, The Netherlands
[121]Res. Group of Paleoclimate & Paleoenvironment, Res. Centr. for Climate and Atmosphere, National Research and Innovations Agency (BRIN), Republic of Indonesia

Correspondence to: Miriam Pfeiffer (Miriam.pfeiffer@ifg.uni-kiel.de)

Abstract. Sea surface temperature (SST) variability in the south-eastern tropical Indian Ocean is crucial for rainfall variability in Indian Ocean rim countries. A large body of literature has focused on zonal variability associated with the Indian Ocean Dipole (IOD), which peaks in austral spring. In today's climate, northward shifts of the Tropical Convergence Zone (TCZ) co-vary with the IOD, and it is unclear whether these shifts may also occur independently. We have developed a new, monthly resolved Sr/Ca record from a sub-fossil coral cored at Enggano Island (Sumatra, Indonesia). Core sections containing diagenetic phases are omitted from the SST reconstruction. U/Th dating shows that the Sr/Ca-based SST record extends from 18618698-19187 and from 18243-18621 with a relative age uncertainty of ±32.4 years (2σ). At Enggano Island, coastal upwelling and cooling in austral spring impacts SST seasonality and is coupled to the latitudinal position of the TCZ. The sub-fossil coral indicates an increase in SST seasonality between 18565 and 19187 relative to the 1930-2008 period. We attribute this to enhanced cooling due to stronger SE winds driven by a northward shift of the TCZ in austral spring. A nearby sediment core indicates colder SSTs and a shallower thermocline prior to ~1930. These results are consistent with an increase in the North-South SST gradient in the eastern Indian Ocean calculated from historical temperature data, that is not seen in the zonal SST gradient. We conclude that the relationship between meridional and zonal variability in the eastern Indian Ocean is non-stationary and modulated by the long-term evolution of temperature gradients.

Formatiert: Hochgestellt

1 Introduction

Sea surface temperature (SST) variability in the south-eastern (SE) tropical Indian Ocean is crucial for rainfall variability in Indian Ocean rim countries (Weller et al., 2014; Cai et al., 2013). A large body of literature has focused on the Indian Ocean Dipole (IOD) (Saji et al., 1999; Webster et al., 1999; Ummenhofer et al., 2009a; Ummenhofer et al., 2009b; Cai et al., 2013; Saji and Yamagata, 2003; Behera et al., 2005; Ashok et al., 2003; Abram et al., 2020), a zonal mode characterized by a reversal of the east-west SST gradient in the tropical Indian Ocean, causing droughts in Indonesia and Australia, and enhanced rainfall and flooding in equatorial East Africa (Ummenhofer et al., 2009a; Ummenhofer et al., 2009b; Saji et al., 1999; Behera et al., 2005; Ashok et al., 2003). Comparatively little attention has been paid to meridional (North-South) SST gradients and related circulation anomalies over the SE tropical Indian Ocean in austral spring, although these can also induce significant droughts in Indonesia, and flooding in southern India and Sri Lanka (Weller and Cai, 2014; Weller et al., 2014). An stronger North-South SST gradient in September-November shifts the southern boundary of the Tropical Convergence Zone (TCZ; see Geen et al. (2020)) northwards (Weller et al., 2014; Weller and Cai, 2014) (Fig. 1, Fig. A1).

The eastern Indian Ocean north of 10°S features the most intense atmospheric convection in the Indian Ocean basin (Fig. 1, Fig. A1) (Schott et al., 2009). In austral spring, meridional displacements of the TCZ are driven by ocean-atmosphere interactions in the SE tropical Indian Ocean, which include monsoon-induced coastal upwelling in September-November and active SST-thermocline feedbacks (Susanto et al., 2001; Webster et al., 1999; Cai et al., 2013; Saji and Yamagata, 2003; Weller et al., 2014). Coastal upwelling is driven by strong, southeasterly (SE) winds along the coasts of Java and Sumatra associated with the South Asian Summer Monsoon (Susanto et al., 2001) (Fig. 2, Fig. A2). Anomalously strong SE winds enhance coastal upwelling and cooling, which may shift the southern boundary of the TCZ to the north of 5°S, and in extreme cases, to the equator (Fig. 1, Fig. A1). The cooling in the SE equatorial Indian Ocean may trigger a reversal of the zonal SST gradient in the tropical Indian Ocean and the development of a positive IOD (pIOD) event (Saji et al., 1999; Fischer et al., 2005). In the satellite era, the occurrence of pIOD events and northward displacements of the southern boundary of the TCZ are tightly coupled (Weller et al., 2014; Weller and Cai, 2014) and the latter may be seen as a characteristic of pIOD events (Fig. 1). However, future projections suggest that northward shifts of the southern boundary of the TCZ may uncouple from the IOD due to the rapidly warming Asian landmass in response to greenhouse warming and, as a result, faster warming rates in the north-eastern Indian Ocean relative to the south-east (Weller and Cai, 2014; Weller et al., 2014). This could induce extreme northward shifts of the TCZ that are not associated with an increased frequency of pIOD events (Weller et al., 2014).

SST variability in the SE equatorial Indian Ocean is poorly represented in historical, gridded data of SSTs, which do not adequately capture the non-linear ocean-atmosphere feedbacks in the region (Yang et al., 2020; Pfeiffer et al., 2022; Cai et al., 2013). Therefore, observational studies on the relationship between meridional and zonal SST variability are limited to the last ~40 years in which we have satellite data of SST (Weller et al., 2014; Weller and Cai, 2014). Coral Sr/Ca ratios measured at monthly resolution were shown to provide a realistic representation of SST variability in the SE tropical Indian Ocean, as, unlike historical SSTs interpolated from sparse data, the coral proxy data is not compromised by non-linear ocean-atmosphere feedbacks (Yang et al., 2020; Pfeiffer et al., 2022; Cahyarini et al., 2021). To date, however, coral studies of historical variability in the SE tropical Indian Ocean have mainly focused on zonal variability associated with the IOD (Abram et al., 2015; Abram et al., 2008; Abram et al., 2007; Abram et al., 2020).
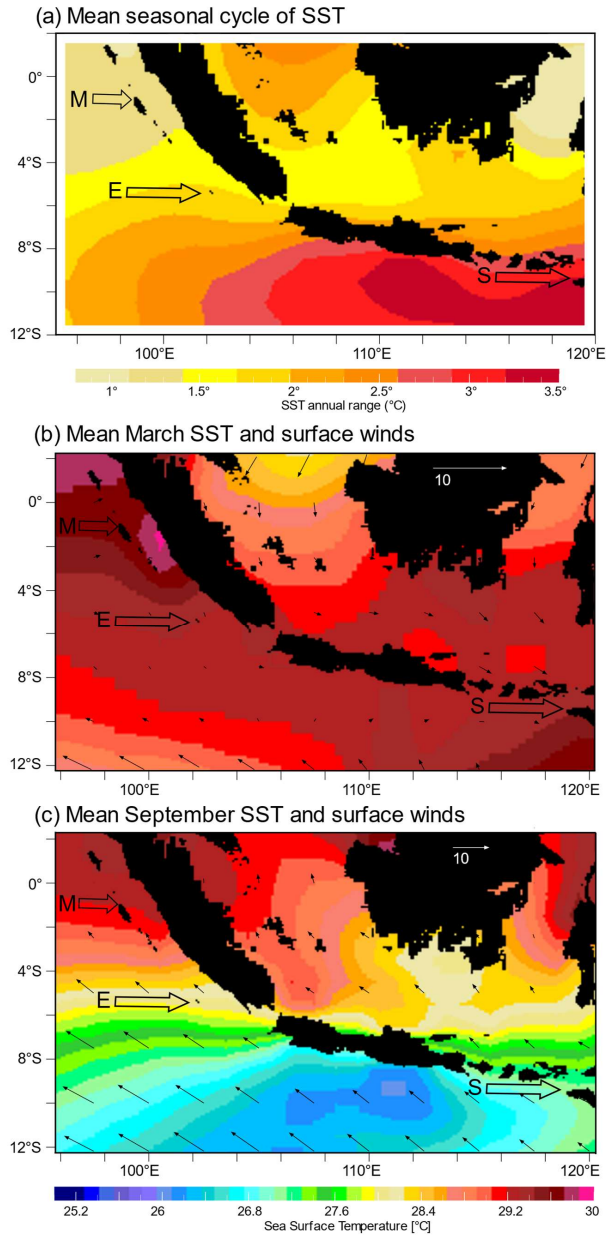
Here, we present a new, monthly-resolved Sr/Ca record from a sub-fossil *Porites* coral drilled at Enggano Island (Sumatra, Indonesia). Our new coral Sr/Ca record derives from a large massive colony found in a dead, partially bio-eroded reef (Fig. 3). U/Th dating indicates that the base of the coral record is 18243 ±32.4 (2σ) years old and the youngest sections extend to the early 20th century. Extensive screening with a state-of-the-art Hitachi SU 3900 Scanning electron microscope (SEM) was performed to identify and omit intervals with minor early marine diagenesis and to ensure the reliability of the Sr/Ca data. Combining our new coral data with previously published coral Sr/Ca records from Enggano Island that extend from 1930-

2008 (Pfeiffer et al., 2022), we investigate the relationship between meridional and zonal SST variability in the SE Indian Ocean prior to the satellite era
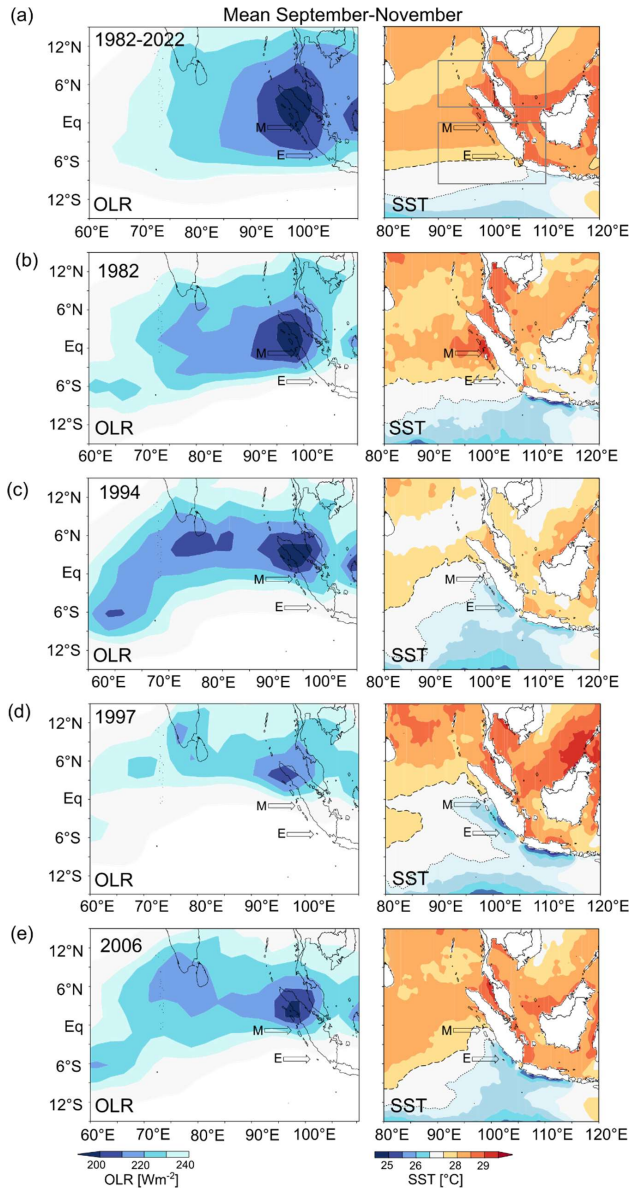
Figure 1: Austral spring outgoing longwave radiation (OLR) and SST in the eastern Indian Ocean. (a) Mean September-November OLR (left) (Schreck et al., 2018) and AVHRR OI SST (right) (Huang et al., 2021) from 1982-2022. (b) September-November OLR (left) and SST (right) for the moderate pIOD event of 1982. (c) Same as (b) for the extreme pIOD event of 1994 (d) Same as (b) for the extreme pIOD event of 1997, (e) same as (b) for the extreme pIOD event of 2006. OLR ≤ 240 Wm⁻² countour (light blue) indicates the boundaries of the TCZ. Note the close correspondence of the 27 °C (stipled) and 28 °C (dashed) countours off the coast of Sumatra and the southern boundary of the TCZ. Arrows mark location of Enggano (E) and Mentawai (M). Grey boxes in (a) indicate area of NE (2.5-7.5 °N, 90-110 °E) and SE (0-10 °S, 90-110 °E) Indian Ocean SST indices used to calculate the North-South SST gradient in the eastern Indian Ocean as in Weller and Cai (2014) and Weller et al. (2014). Charts computed at the knmi climate explorer (https://climexp.knmi.nl).

(a) Mean seasonal cycle of SST

(b) Mean March SST and surface winds

(c) Mean September SST and surface winds

Figure 2: SST seasonality and surface winds in the SE Indian Ocean. (a) The amplitude of the mean seasonal cycle of SST (in °C) decreases from >3 °C to 1 °C from Java to Sumatra. (b) In austral fall, mean SSTs (colors) are warm and uniform, and surface winds (vectors) are weak. (c) In austral spring, strong, alongshore SE winds (vectors) lead to cooling off the coast to Java and Sumatra, and large meridional differences in mean SSTs (colors). Open arrows in (a) and (b) mark location of Enggano (E), northern Mentawai (M), and Sumba Island (S). Note the steep austral spring SST gradients around Enggano. SST data from OI SST (Reynolds et al., 2002), wind data from (Kalnay et al., (1996). Charts computed at https://iridl.ldeo.columbia.edu/.

4

2 Study area

Enggano Island lies ~200 km off the coast of south-eastern Sumatra at 5.22 °S, 102.14 °E (Fig. 3). It is the southernmost island on the fore-arc ridge offshore Sumatra, which also comprises the Mentawai Island chain located further north (3-1 °S, 98-100 °E). In austral spring, SE winds associated with the South Asian summer monsoon generate coastal upwelling and cooling off Java and Sumatra (Fig. 2) (Susanto et al., 2001). The standard deviation of monthly mean SST reveals the centers of upwelling (Fig. 3, Fig. A2). Upwelling first develops off the coast of Java in June, and then propagates north-westwards (Fig. A2). It reaches Enggano in July, and extends to the northern Mentawai Islands in October (Fig. A2). In November-December, westerly winds terminate coastal upwelling and SE Indian Ocean SSTs are generally warm with comparatively little spatial variability in austral fall (Fig. 2).

The strength of the SE winds in austral spring thus primarily determines the seasonal cycle of SSTs in the SE Indian Ocean, seen in a decrease of seasonality, from > 3 °C off Java to ~1.5-1.0 °C off Sumatra, which reflects spatial variations in the frequency of occurrence of coastal upwelling and cooling in September-November (Fig. 2, Fig. 3). At Enggano, austral spring SSTs are colder than at the northern Mentawai Islands, SST seasonality is larger, and annual mean SSTs are lower (Fig. 2, Fig. 3). Furthermore, Enggano Island is situated in a region where the magnitude of cooling during the SE monsoon (and, as a result, the amplitude of the mean seasonal cycle) changes profoundly over short distances (Fig. 2). This means that relatively small changes in the strength/extend of the SE winds should be seen in the magnitude of austral spring cooling and the amplitude of the mean seasonal cycle at Enggano Island.

Off the coast of Java, the SE winds cause strong upwelling and cooling every year (Susanto et al., 2001), and mean September-November SSTs are low (<27 °C) (Fig. 2, Fig. 3). On interannual time scales, stronger-than-normal SE winds lead to an anomalous strengthening of coastal upwelling and cooling off Sumatra that may lead to (I) a northward shift of the southern boundary of the TCZ in austral spring (Fig. 1, Fig. A1) (Weller et al., 2014), (II) a reversal of the zonal SST gradient in the tropical Indian Ocean and the development of a pIOD event (Saji et al., 1999; Yang et al., 2020; Ng et al., 2015). During extreme pIOD events, the southern boundary of the TCZ shifts to the north of 5°S (Weller et al., 2014), i.e. to the north of Enggano Island. In these years, cool SSTs down to 25 °C can reach the equator (Fig. 1, Fig. A2). The occasional occurrence of extreme pIOD events in an equatorial region featuring warm surface waters in normal years is reflected in a strong negative skewness of September-November SSTs off Sumatra (Fig. 3) (Yang et al., 2020) and an enhanced seasonal cycle in these years. In contrast, anomalous austral spring cooling during moderate pIOD events is weaker and spatially restricted to the south-eastern coast of Sumatra, where Enggano is located, and the Java and Timor Sea (Fig. 1, Fig. A2). In addition to IOD-related SST variability (Pfeiffer et al., 2022), the corals from Enggano Island should therefore be sensitive recorders of changes in the strength of the SE winds and the latitudinal position of the southern boundary of the TCZ (Fig. 1, Fig. 2, Fig. A1).
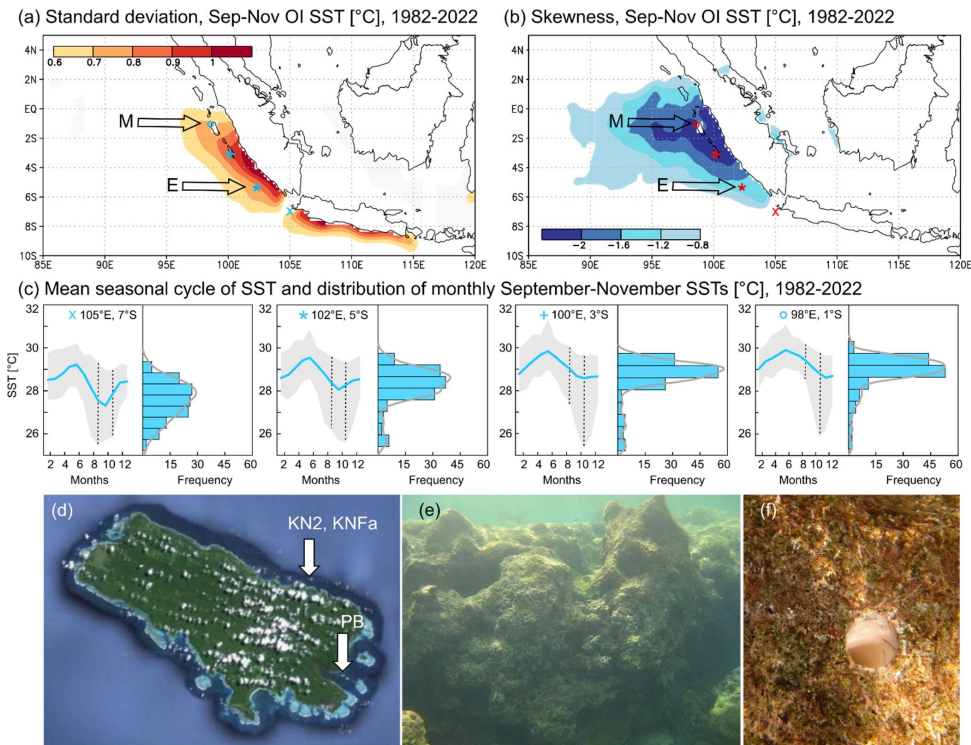
5

Figure 3: Location and climatic setting of Enggano Island. (a) The standard deviation of September-November SST indicates areas of coastal upwelling off the coast of Java and Sumatra. (b) The skewness of September-November SSTs reflects interannual coastal upwelling events. Arrows in (a) and (b) mark location of Enggano Island (E) and northern Mentawai Island (M). Charts were
135 **computed at the knmi climate explorer (https://climexp.knmi.nl). (c) Mean seasonal cycles of satellite SST (thick blue lines) from northern Java to central Sumatra with 99 % confidence levels (grey shading). SST grids are selected with a latitudinal spacing of 2°, symbols indicate their position in (a) and (b). Histograms show the distribution of monthly mean SSTs in the September-November season. At all sites, SST minima are ~25 °C, but progressively higher mean September-November SSTs occur at sites north of 7°S, where only extreme pIOD events cause intense coastal upwelling. The resulting negative skewness is indicated by the**
140 **99% confidence levels around the September-November SSTs (dashed black lines), and seen in the histograms of mean September-November SSTs. Histograms were computed using PAST (Hammer et al., 2001). SST data is from AVHRR OI SST (1/4° grids) (Huang et al., 2021). (d) Satellite image of Enggano Island showing the fringing reefs surrounding the Island from GoogleEarth. At its longest section, Enggano Island is 35 km long. Modern cores were drilled at the southeastern (PB: 5°27.888'S, 102°22.218'E) and northeastern (KN2: 05°21.713'S, 102°21.511'E) coast. A subfossil coral (KNFa) was drilled next to core KN2. (e) Dead reef on the**
145 **northeastern coast of Enggano Island and (f) bio-eroded surface of sub-fossil coral colony with open borehole with a diameter of 4 cm. Photos from S.Y. Cahyarini.**

3 Methods and data

3.1 Coral collection

In an August 2008 field campaign, sub-fossil, dead fringing reefs were discovered around Enggano Island (Sumatra, Indonesia)
150 in a water depth of ~3m (Fig. 3). A large massive *Porites* coral was found and a 1.83 m coral core (KNFa) was drilled using a pneumatic drill powered by Scuba tanks. After drilling, the core KNFa was cut into 5 mm thick slabs and prepared for subsampling following standard procedures (Cahyarini et al., 2014b). X-rays (Fig. 4) and luminescence scans (Fig. A4) were made at the Royal Netherlands Institute for Sea Research (NIOZ) on untreated coral slabs to reveal the coral's seasonal banding pattern and to indicate potential zones of diagenesis. The KNFa core shows multiple density bands per year that do not allow

6

155   a precise chronology based on annual bands, but a good correlation of corresponding sections on adjacent coral slabs (Fig. 4, Fig. A4).

Two modern *Porites* corals (KN2 and PB) were collected from living corals during the same field campaign, and their Sr/Ca records were published previously (Pfeiffer et al., 2022). The two modern corals extend from 1930-2008, and are used here for comparison with the sub-fossil coral data. See Figure 3 for the exact location of the coral cores.

160   **3.2 Diagenetic screening**

Based on X-ray images and luminescence scans (Fig. 4, Fig. A4), potential diagenetic alteration was assessed, using representative samples for mineralogical and microscopic analysis. Conventional, destructive analysis, including powder X-ray diffraction (XRD, n=3), thin-section (n=3) and scanning electron microscopy (SEM, n= 5) on gold-coated coral blocks (see Fig. 4 for sample location) were carried out.

165   Furthermore, we conducted higher resolution, non-destructive mineralogical and microscopic analysis directly on the coral slabs, parallel to the proxy sampling tracks. The 2-D-XRD system Bruker D8 ADVANCE GADDS was used for non-destructive XRD point-measurements with a calcite detection limit of ~ 0.2 % (Smodej et al., 2015). The nineteen 2-D-XRD measurements resulted in a sampling resolution of one spot analysis every ~ 7 cm. Sections showing a mottled appearance on the luminescence scans were selected for non-destructive SEM analysis with the Hitachi SU3900 system. The extra-large

170   chamber of this SEM system can accommodate coral slabs up to 30 cm in length (Fig. A5, A6). The analyses were carried out in low vacuum mode (30 and 50Pa) using an ultra-variable-pressure detector (UVD) and a backscattered electron detector (BSE). This low vacuum mode allows the coral slabs to be analyzed continuously and directly along the proxy sample track without the need for coating with conductive materials such as gold.

7
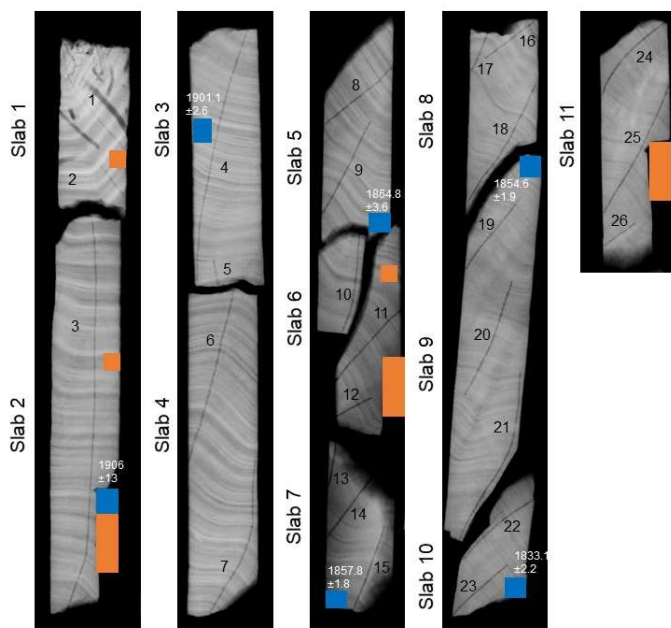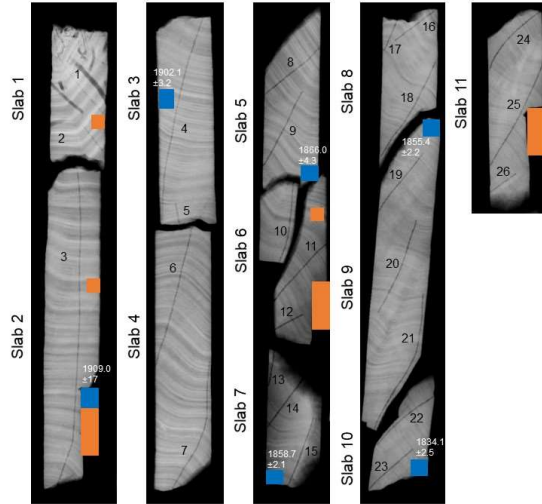
175 **Figure 4: X-ray image of the sub-fossil coral core KNFa from Enggano Island. Core slabs and sampling transects for Sr/Ca analysis are numbered (data see Fig. 5). Blue squares indicate samples taken for U/Th dating and their ages. Note: the core shows prominent sub-annual bands that allow a good match between different slabs. Some sections of the core were cut off to assess preservation using conventional, destructive methods (powder XRD, thin section and SEM analysis using gold-coated stubs of coral). Small orange boxes indicate locations for SEM samples. Large orange boxes indicate locations for combined powder-XRD, SEM and thin-section**
180 **samples. See text for discussion.**

3.3 Sr/Ca analysis

The KNFa core was subsampled for Sr/Ca analysis at 1 mm intervals, i.e. at approximately monthly resolution. For each subsample, we extracted 0.1-0.2 mg of coral powder for Sr/Ca analysis using a hand-held drill. Sr/Ca ratios were measured at Kiel University using a Spectro Ciros CCD SOP inductively coupled plasma optical emission spectrometer (ICP-OES).
185 Elemental emission signals were simultaneously collected and subsequently processed following a combination of techniques described by (Schrag, (1999) and (Villiers et al., (2002). Average analytical precision of Sr/Ca measurements as estimated from sample replicates was typically around 0.08 % RSD or less than 0.1 °C (n > 180). All coral Sr/Ca ratios were normalized to an in-house standard calibrated against JCp-1 (8.838 mmol mol^{-1}) (Hathorne et al., 2013). Measurements of JCp-1 had a median of 8.832 mmol mol^{-1}, and a standard deviation of 0.009 (1σ) or 0.10 % RSD.
190 The chronology of the coral Sr/Ca records presented in this study is developed by assigning mid-September (on average the coldest month) to the Sr/Ca maxima. The data is then linearly interpolated to 12 monthly values per year. Average coral growth rates estimated from trace element data are larger than 10 mm/year in all cores (Table A1).

3.4 U/Th Dating and chronology

The age of KNFa was estimated by U/Th dating at National Taiwan University, following the methods of (Shen et al., (2012).
195 After chemical separation for U and Th isotopes in a clean room, the samples were analysed with a multi-collector inductively coupled plasma mass spectrometer (MC-ICP-MS, NEPTUNE). Results are shown in Table A2.

A floating chronology was estimated following the approach of Domínguez-Villar et al. (2012) (Fig. A7). The age of the coral record was estimated from the intercept of the linear regression between the U/Th ages and the annual cycles of Sr/Ca (Fig. 5), assuming that the slope of this regression is one, using Eq. 1:

200 $No. of\ annual\ cycles = U - Th\ age * m + b$, (1)

8

where "b" is the floating age. With this regression, the differences between U/Th ages and corresponding Sr/Ca ages are minimal (0.1 years for the overall time series). The age uncertainty of the floating chronology was estimated with a Monte Carlo approach (20,000 loops) using the 2σ U/Th error. The base of the KNFa Sr/Ca record is dated to 1824̶3̶ ± 3̶2̶.4 (2σ) years CE.

205 Combining the U/Th ages with the coral density banding and growth rates suggest that the coral died in the early 1930s, although the exact timing cannot be determined due to extensive bioerosion at the top of the coral. It is unclear what caused the death of the sub-fossil coral (and the fringing reef where the core was taken), but possible candidates include several major earthquakes centered on Enggano island in the 1930s with magnitudes $\geq$ 7 (Newcomb and McCann, 1987), or severe cold anomalies, possibly coupled with red tides, due to extreme IOD-induced upwelling events (Abram et al., 2003).

210 **3.5 Coral Sr/Ca-SST conversion**

To avoid biases from so-called 'vital effects' that affect mean coral Sr/Ca ratios (e.g. Cahyarini et al., 2011; Ross et al., 2019), all coral Sr/Ca records were centered to their mean and converted to SST units assuming a coral Sr/Ca-SST relationship of -0.06 mmol mol^{-1} per 1 °C (Corrège, 2006; Ross et al., 2019; Watanabe and Pfeiffer, 2022), hereafter referred to as SST$_{center}$. This slope is consistent with the coral Sr/Ca-SST calibrations of the two modern corals KN2 and PB from Enggano Island

215 with satellite SST data (Pfeiffer et al., 2022), which is available since 1982. SST$_{center}$ inferred from KN2 and PB Sr/Ca data shows the same distribution as satellite SSTs in the grid including Enggano Island (Pfeiffer et al., 2022) (Fig. A8).

3.6 Statistics

Distributions were visualized and compared using PAST (Hammer et al., 2001). Histograms, box- and violin-plots were
220 calculated using measured Sr/Ca data prior to processing, and compared with interpolated, monthly Sr/Ca data and SST$_{centre}$ inferred from coral Sr/Ca ratios. As age model development/interpolation does not influence the spread of measured Sr/Ca data, this allows a comparison between raw and processed Sr/Ca records. The distribution of SST$_{centre}$ inferred from coral Sr/Ca was compared to satellite SST (centered to its mean) using histograms, box- and violin-plots, again circumventing potential mis-alignments arising from uncertainties of sub-seasonal age assignments. To test for equality of distributions, we used the
225 two-sample Kolmogorov-Smirnov-test in PAST (Hammer et al., 2001). Means were compared using a two-sided students t-test in PAST (Hammer et al., 2001).

Mean seasonal cycles of SST were calculated from the coral data by averaging the monthly SST$_{centre}$ records. The uncertainties of this 'coral climatology' were calculated using a Monte Carlo approach based on an R script (R core team, 2023) developed by Watanabe and Pfeiffer (2022) and expanded in Zinke et al. (2022), and include the analytical uncertainties of the Sr/Ca
230 measurements (0.08 %RSD for monthly values) and the calibration uncertainty of the Sr/Ca-SST slope (±0.01 mmol/mol per 1°C) in addition to the spread of the monthly mean data.

Wavelet Power Spectra (Torrence and Compo, 1998) were calculated using the "biwavelet" package and the R software (R core team, 2023). All wavelet analyses were based on the Morlet Wavelet. The significance of power spectra was tested using the $\chi 2$ test with a 95% significance level. The Mann-Kendall test was carried out to test the significance of trends using R
235 software (R core team, 2023). The trend change point (Toms and Lesperance, 2003) was estimated using the "SiZer" package (Chaudhuri and Marron, 1999) in R (R core team, 2023). The 95% confidence level of trend change point was generated based on a bootstrap test (n = 1000).

9

4. Results

4.1 Coral preservation

240 The three conventional powder and nineteen 2D-XRD-analysis (see Fig. 4 for location) indicate that the subfossil core KNFa is purely aragonitic and does not contain any calcitic phases. The analyses of the conventional SEM samples and thin-sections (see Fig. 4 for location) indicates a generally excellent preservation with pristine, smooth skeletal surfaces, except for the SEM sample near the top of the coral core, which shows minor (< 5 µm-long) but pervasive aragonite cementation. To evaluate the extent of potential diagenetic alteration we scanned the entire length of the Sr/Ca sampling tracks on slabs 1 and 2, using the

245 uncoated coral slabs (see Methods and Fig. A5, A6). This analysis confirmed that minor fibrous aragonite cements (5 to 10 µm long) and incipient dissolution are restricted to the upper ~ 14 cm of the coral core, which also shows abundant bioerosion traces (Fig. 4: Slab 1), and a dull to mottled appearance in luminescence scans (Fig. A4). We therefore subsequently used the SEM to scan all core intervals that show similar dull colors in luminescence scans. After the proxy measurements, we additionally checked all intervals containing prominent Sr/Ca anomalies for diagenetic changes based on SEM observations

250 directly on the coral slabs. Using this method, we were able to identify patches of aragonite needle cements (5 to 10 µm long) (Fig. A6), that had escaped detection with our previous standard screening protocol. Sr/Ca data from all intervals showing patchily distributed aragonite cements (sampling transects 1, 2, top of 3, base of 9 to top of 15, see Fig. 4 and 5) were excluded from further interpretation, since even light levels of aragonite cementation may lead to higher bulk Sr/Ca-values and consequently a cold bias in temperature reconstructions (Enmar et al., 2000; Allison et al., 2007; Hendy et al., 2007; Sayani et

255 al., 2011).

4.2 The sub-fossil coral Sr/Ca record

Figure 5 shows the coral Sr/Ca data as measured along the maximum growth axis of core KNFa, prior to interpolation to monthly values and prior to omitting intervals affected by diagenesis. Therefore, each dot represents one Sr/Ca measurement of a discrete subsample. Also indicated are the slabs of the coral core and the sampling transects of Sr/Ca analysis (in color,

260 numbers of slabs and transects are also shown on the x-ray images, see Fig. 4). Data from overlapping transects are shown on top of each other. The first Sr/Ca measurement on each new slab is marked as 'slab boundary'; note that this data overlaps with data from the previous slab due to the coral's growth. After measuring the Sr/Ca ratios along the entire core at 1 mm intervals, we subsequently omit data from transects where early marine diagenesis was detected by non-destructive SEM analysis from further processing (see 'coral preservation'). These sections are masked out in grey in Figure 5.

265 In the intervals not affected by diagenesis, the Sr/Ca record of KNFa shows clear seasonal cycles which can be counted visually to develop an age model. By combining this internal coral chronology with the U/Th ages (see methods), we estimate that the KNFa Sr/Ca record extends from 1824~~3~~-1862~~1~~ and ~~1861~~8698-1918~~7~~ (Fig. A7, A9, Fig. 6), i.e. it encompasses a total of 94 years with 87 years of record, with a relative age uncertainty of ±~~3~~2.4 years (2σ). The Sr/Ca data from well-preserved sections of the core show an excellent reproducibility between sampling transects (note that slight offsets along the X-axis reflect

270 differences in coral growth), i.e. the means and variations of measured Sr/Ca ratios are consistent throughout the core (Fig. 5). The distribution of the measured Sr/Ca data of KNFa is investigated in intervals representing approximately equal amounts of data points. The Sr/Ca distribution is symmetric with a standard deviation of 0.05 to 0.053 mmol mol^{-1} in the upper sections of the coral core (slab 3 to top of slab 8), symmetric with a standard deviation of 0.035 mmol mol^{-1} from slab 8 to 9, and positively skewed with a standard deviation of 0.044 mmol mol^{-1} from slab 10 to 11. Note, however, that the positive skewness

275 of Sr/Ca data from slab 10 and 11 is due to only four consecutive Sr/Ca data of up to 9.148 mmol mol^{-1} on slab 11 (which cannot be attributed to diagenesis). The reduction in standard deviation is due to a persistent change in the nature of the Sr/Ca record that occurs ~850 mm below the top of the coral (Fig. 5).
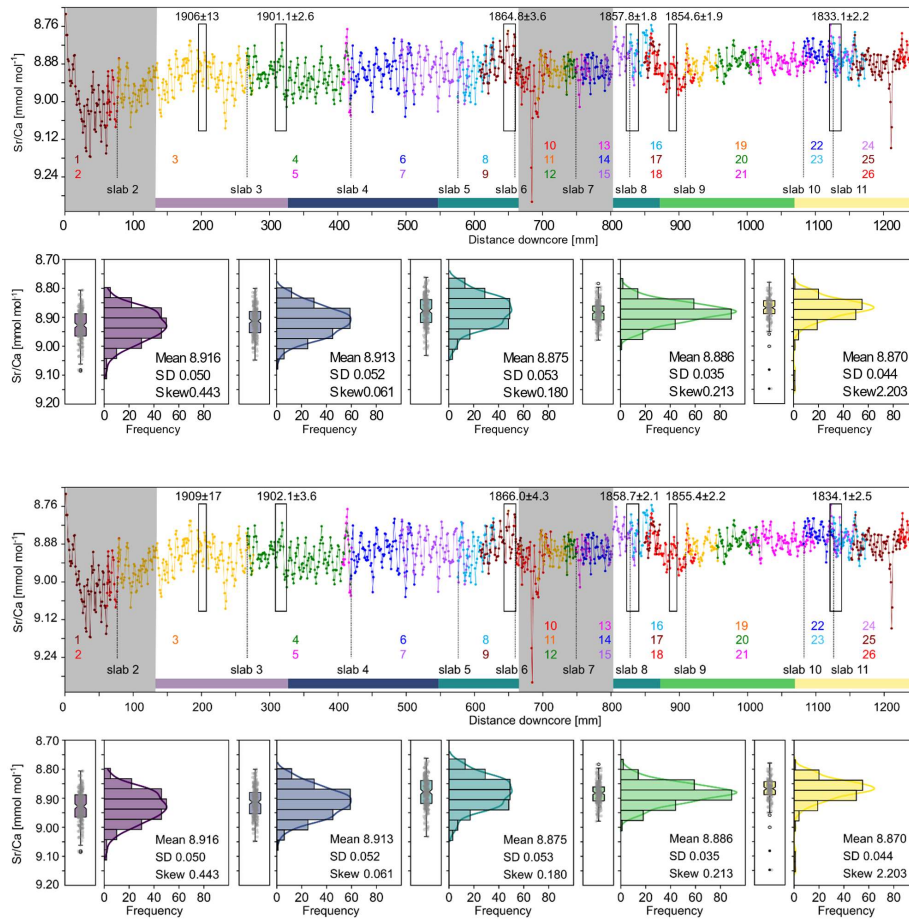
10

Figure 5: Sub-fossil coral Sr/Ca data of core KNFa. Top panel: Measured Sr/Ca data of core KNFa vs. distance downcore (in mm).
Each dot corresponds to one Sr/Ca measurement. Sampling transects are highlighted by different colors and numbered (bottom)
(see Fig. 4 for location of transect). Grey shading marks intervals discarded from further interpretation as diagenetic alterations
have been detected. Sections sampled for U/Th ages are shown by black rectangles. Color bars at the bottom indicate data included
in the histograms, box- and jitter-plots shown in the bottom panel. Note the reduction in the standard deviation of measured Sr/Ca
data at a depth of ~860 mm. Histograms computed using PAST (Hammer et al., 2001).

5. Discussion

5.1 Sub-fossil coral Sr/Ca data and diagenesis

Sub-fossil corals are an important archive to extent the instrumental record back into pre-industrial periods (Abram et al., 2020; Cobb et al., 2013; Sanchez et al., 2020). Living corals may grow continuously for more than 300 years (Zinke et al., 2004; DeLong et al., 2013; Linsley et al., 2000), but in many key regions of climate variability, extreme climate disturbances can contribute to their demise (Abram et al., 2003). However, applying the coral Sr/Ca thermometer to sub-fossil corals is challenging as relatively minor amounts of diagenetic alteration can already significantly distort the Sr/Ca thermometer (Allisson et al. 2007; (Sayani et al., 2011; Sayani et al., 2022). Standard screening protocols based on destructive analysis of

discrete samples by thin-section, XRD and SEM are not always sufficient to map out the often patchily distributed diagenetic phases in corals. In this study, only the diagenetic alteration at the top of the core was identified using conventional methods, while other patches of aragonite cements in slabs 5 to 7 were not detected. A way to circumvent this problem are non-destructive methods that can be used to screen coral slabs for diagenetic phases at high spatial resolution (Murphy et al., 2017).

300 2D-XRD analysis non-destructively quantifies the amount of calcite cements directly on the coral slab with mm-scale spatial resolution (Smodej et al., 2015; Leupold et al., 2021). However, other types of diagenetic alteration such as aragonite dissolution or aragonite cements cannot be detected by XRD (Allison et al., 2007; McGregor and Abram, 2008). Typically, aragonite cements are patchily distributed (Nothdurft and Webb, 2009; (Sayani et al., 2011; Sayani et al., 2022; Smodej et al., 2015), while adjacent areas of the coral's skeleton are unaffected (Zinke et al., 2016). Such local concentrations of diagenetic

305 phases could introduce spikes in the Sr/Ca data or other proxy records, that could be misinterpreted as climate events (Quinn and Taylor, 2006). Use of an SEM with an extra-large chamber in combination with an ultra-variable pressure detector (Fig. A5), allowed us to scan entire core slabs along the proxy sampling tracks without the need for a conductive coating. Our record showed an extreme spike with a Sr/Ca ratio of 9.32 mmol mol^{-1} on transect 10 of slab 6 (Fig. 5). We were able attribute this extreme Sr/Ca spike to a patch of aragonite cement and to omit this 'false alarm' spike from further interpretation. This is

310 important as at Enggano Island, such a spike would indicate an extreme pIOD event with a cooling exceeding -5 °C. Events of this magnitude do not occur in recent time periods captured in the satellite record, and including this Sr/Ca data would have significantly impacted the climatic interpretation of core KNFa. Furthermore, the interval from the base of transect 9 to the top of transect 15 lacks clear seasonal variability in coral Sr/Ca, which is normally indicative of irregularly distributed patches of diagenetic cements impacting the Sr/Ca proxy, but since Enggano Island lies in a region with low seasonality, confirmation by

315 SEM is important to map the extend of this zone. We conclude that it is important to clearly identify and delimit zones of even minor, early marine diagenesis in young, sub-fossil corals, preferable directly adjacent to the sampling transect of Sr/Ca analysis, as a basis for a subsequent climatic interpretation of the Sr/Ca data from sub-fossil corals (Sayani et al., 2022).

5.2 SST$_{center}$ inferred from Enggano coral Sr/Ca data since 182~~4~~3

Two modern coral Sr/Ca records (KN2 and PB) from Enggano Island were shown to closely track satellite SSTs that extend

320 back to 1982 and to reliably record IOD variability, while gridded SST products interpolated from sparse historical data systematically underestimated extreme pIOD events, even in the time period covered by satellites (Yang et al., 2020; Pfeiffer et al., 2022). This has been attributed to non-linear ocean atmosphere feedbacks in the south-eastern equatorial Indian Ocean that are not captured in the statistical methods used to interpolate historical SSTs from sparse observational data (Ng et al., 2015; Yang et al., 2020).

325 In this study, we re-evaluate the two single-core modern coral Sr/Ca records as a basis for the interpretation of the sub-fossil KNFa Sr/Ca record. We limit the interpretation of KNFa on aspects clearly seen in each single modern coral record. Figure A9 compares the coral Sr/Ca records of the two modern corals from Enggano Island with the sub-fossil record of KNFa after interpolation to monthly resolution. The most notable feature of the two modern coral Sr/Ca records are large positive Sr/Ca anomalies during the extreme pIOD events of 1961, 1963, 1967, 1994, 1997 and 2006 (Fig. A9, Fig. 6) (Pfeiffer et al., 2022).

330 Violin and box plots of the monthly Sr/Ca data from each Enggano coral record are computed in time intervals spanning approximately 20 years (note that some variations arise from the total length of the time periods covered by the coral records). The median Sr/Ca ratios of KN2 and PB are offset by ~0.065 ~~by~~ ±0.0156 mmol mol^{-1} (1σ) (Fig. A9), which would correspond to a difference >1 °C assuming a Sr/Ca-SST relationship of -0.06 mmol mol^{-1} °C^{-1} (Corrège, 2006; Watanabe and Pfeiffer, 2022), if temperature related. However, offsets in mean or median coral Sr/Ca ratios from different coral colonies are likely

335 due to so-called 'vital effects' (Villiers et al., 1994; Watanabe and Pfeiffer, 2022; Ross et al., 2019) and have been seen even in coral Sr/Ca records from adjacent colonies growing next to temperature loggers (Leupold et al., 2019). For climate reconstructions from corals, it is important that this offset remains constant within a coral core, which has been demonstrated

in numerous calibration studies (Ross et al., 2019). The constant difference in median Sr/Ca ratios between KN2 and PB supports the use of Enggano coral Sr/Ca ratios as indicators of SST variability (Fig. A9).

340 Both modern coral cores show similar distributions of monthly Sr/Ca data in each ~20-year time interval, with a strong positive skewness in time periods with extreme pIOD events (1950-1969; 1990-2008) and a symmetric distribution in periods without extreme pIOD events (Fig. A9). This includes the number and spread of outliers (which reflect extreme pIOD events). The KNFa record, in contrast, shows symmetric distributions, albeit with a larger spread around the median (indicating a larger standard deviation of the Sr/Ca data) in all time windows between 1865-1918. This is also seen in the raw, un-interpolated

345 Sr/Ca data of KNFa (Fig. 5). Between 1824 and 1855, the spread of coral Sr/Ca around the median reduces again to ranges seen in the modern cores, with outliers arising from a few extreme positive Sr/Ca values in 1826 indicating an extreme pIOD event. The reduction in the standard deviation prior to 1865 is also seen in the raw, un-interpolated Sr/Ca data of core KNFa (Fig. 5).

Recent extreme pIOD events (1961, 1963, 1967, 1994, 1997 and 2006) in the SST_{center} records inferred from KN2 and PB

350 Sr/Ca data each indicate a cooling of ~ -4 °C at Enggano Island (Fig. 6, Pfeiffer et al., 2022). These extreme events also impacted the meridional SST gradient in the eastern equatorial Indian Ocean, with warm anomalies in the north and cold anomalies in the south, causing a northward shift of the southern boundary of the TCZ (Fig. 1, Fig. A10). September-November mean SST_{center} data of KN2 and PB is highly correlated with the meridional SST gradient in the eastern Indian Ocean (Fig. A10).

355 The sub-fossil coral KNFa shows only one large Sr/Ca anomaly in 1826, near the end of the coral record, which is on par with these recent extreme events (Fig. 6). SEM images confirm that the 1826 event cannot be attributed to diagenetic changes and we therefore attribute it to an extreme pIOD event – the only one in the interval from 1824 to 1855 recorded at Enggano Island. Between 1865-1918, KNFa shows several cold anomalies in austral spring (Fig. 6, Fig. A9), the largest of which (1882, 1886, 1890, 1908, 1916) are comparable to 2006, a slightly weaker extreme pIOD event in the modern

360 record (Pfeiffer et al., 2022; Yang et al., 2020).

To better characterize the changes in SST variability inferred from coral Sr/Ca over time, we computed wavelet power spectra. In the two modern records, extreme pIOD events are clearly seen as localized concentrations of power at sub-seasonal to interannual periodicities (Fig. 6). Seasonal variability is not persistent. This changes in the sub-fossil record of KNFa between 1865-1918. In this period, seasonal variability is a persistent signal, while interannual variability is not significant (Fig. 6).

365 Prior to 1865, seasonal variability is again not persistent, and the single extreme pIOD event in 1826 is seen as a localized concentration of power at sub-seasonal to interannual periodicities (Fig. 6). These results suggest changes in the SST variability in the SE Indian Ocean that include changes in seasonality in addition to interannual variability associated with the IOD.
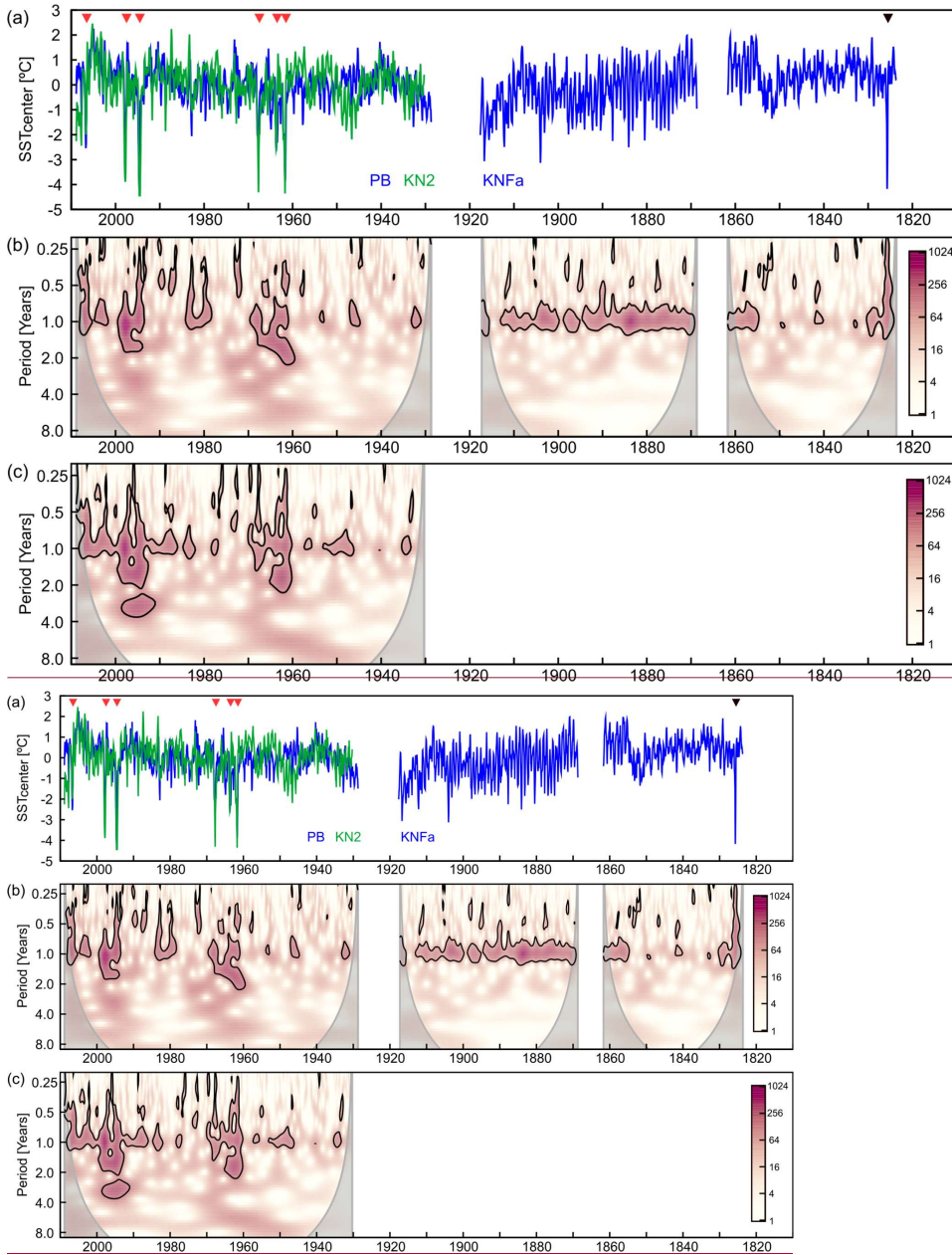
Figure 6: Modern and sub-fossil, monthly SST$_{centre}$ inferred from Enggano coral Sr/Ca ratios. (a) The monthly SST$_{centre}$ record from Enggano comprises two modern (PB, KN2) and one sub-fossil core (KNFa) and extends from 1930-2008, ~~1869~~1869-191~~8~~7 and 182~~43~~- 186~~2~~1. Note that the sub-fossil coral chronology is based on U/Th dating with an age uncertainty of ±~~3~~2.4 years (2σ). Extreme pIOD events lead to cooling of ≥ -4 °C in 1961, 1963, 1967, 1994, 1997 and 2006 (red arrows). The sub-fossil core KNFa shows an extreme pIOD event on par with the event in 1997 in 182~~6~~5 (black arrow). (b) Wavelet power spectra of SST$_{centre}$ time series of core PB and KNFa. (c) same as (b) but for core KN2. Power spectra of PB and KN2 are dominated by extreme pIOD events (red arrows in a). SST$_{centre}$ of KNFa shows enhanced seasonal variability between 185~~6~~5 and 191~~8~~7. Prior to 185~~6~~5, seasonal variability is comparable

14

to PB and KN2. Wavelet Power spectra were computed in R using the Morlet Wavelet. Thick black lines indicate significant periodicities at a certain time (p<0.05). Grey shading indicates cone of influence.

5.3 SST seasonality between 185~~6~~5 and 191~~7~~8

380 The wavelet power spectra (Fig. 6) of the subfossil coral shows persistent SST seasonality between 185~~6~~5 and ~~1917~~1918, while the modern corals (and the sub-fossil coral prior to 185~~6~~5) show localized concentrations of power during extreme pIOD events. To further investigate these changes, we computed mean seasonal cycles of SST_{centre} and their 99 % confidence intervals for the time periods from 1930-2008 (KN2 and PB), 185~~6~~5-~~1917~~1918 (KNFa) and ~~1823~~1824-185~~5~~4 (KNFa) (Fig. 7). Modern SST_{centre} seasonality inferred from coral Sr/Ca varies from 1.1 °C (KN2) to 1 °C (PB) between 1930 and 2008, consistent with

385 satellite data of SST that is available since 1982 (Fig. 7). SST_{centre} seasonality increases to ~1.9 °C between 185~~6~~5-~~1917~~1918 and then decreases again to modern values (~1 °C) between ~~1823~~1824 and 185~~5~~4. The difference in the mean seasonal cycles between 1930-2008 and 185~~6~~5-~~1917~~1918 is statistically significant at the 99% confidence level, while the mean seasonal cycles between 1930-2008 and ~~1823~~1824-185~~5~~4 are statistically indistinguishable (Fig. 7). In the two modern SST_{centre} records from Enggano Island, the extreme pIOD events (1961, 1963, 1967, 1994, 1997 and 2006) cause a strong skewness (Fig. 8, Fig.

390 A8, Fig. A9). This skewness is reflected in the 99 % confidence intervals around September-November mean SST_{centre} in Figure 7, and is also seen in present-day satellite SSTs centered at Enggano Island (Fig. 3).

In contrast, in the time period from 185~~6~~5-~~1917~~1918, when SST_{center} seasonality is enhanced, the distribution of September-November SST_{center} is symmetric (Fig. 7, Fig. 8), and significantly differs from the modern data (based on a Kolmogorov-Smirnov test, see Table A3). In this period, strong September-November cooling occurs in almost every year (Fig. 6). The

395 magnitude of the mean seasonal SST_{center} cycle as well as the distribution of September-November SST_{center} are comparable to satellite SSTs seen today at ~7°S, i.e. off northern Java (Fig. 8, Table A4). Furthermore, maximum SSTs occur 1-2 months earlier than in modern coral SST_{centre} and satellite SSTs, suggesting an early onset of austral spring cooling. Our results suggest stronger SE winds extending further to the northwest along the Java-Sumatra coast, and an expansion of the region with strong wind- and upwelling-induced cooling in austral spring. We therefore believe that the increase in the seasonal cycle of SST_{center}

400 between 185~~6~~5-~~1917~~1918 reflects an earlier onset coupled with an increased strength of the SE winds in July-October, which then penetrated further north along the Java-Sumatra coast in almost every year, and led to stronger cooling at Enggano Island. This would imply a shift in the mean position of the southern boundary of the TCZ to the north of Enggano Island in austral spring, and a northward contraction of the eastern Indian Ocean Warm Pool coupled with a stronger meridional SST gradient (Weller and Cai, 2014; Weller et al., 2014). We favor this interpretation over a change in zonal variability associated with the

405 IOD, as the IOD is by definition an interannual phenomenon of climate variability. At present, pIODs are relatively rare, impacting the 99 % confidence levels around the September-November mean SSTs, rather than the monthly mean values of September-November SSTs (i.e. the mean seasonal cycle itself). Seasonality in the eastern tropical Indian Ocean, including the onset of the SE winds of Java and Sumatra, is primarily driven by the Asian summer monsoon, and changes in the mean state of the monsoon may impact the latitudinal position of the southern boundary of the TCZ in austral spring (Fig. 1, Fig. 2)

410 (Weller et al., 2014). An analysis of the Australian-Asian monsoon using 43-years of ERA-40 data does show long-term trends in onset/retreat dates and duration in each of the two monsoon seasons (Zhang, 2010), suggesting that this scenario is plausible.
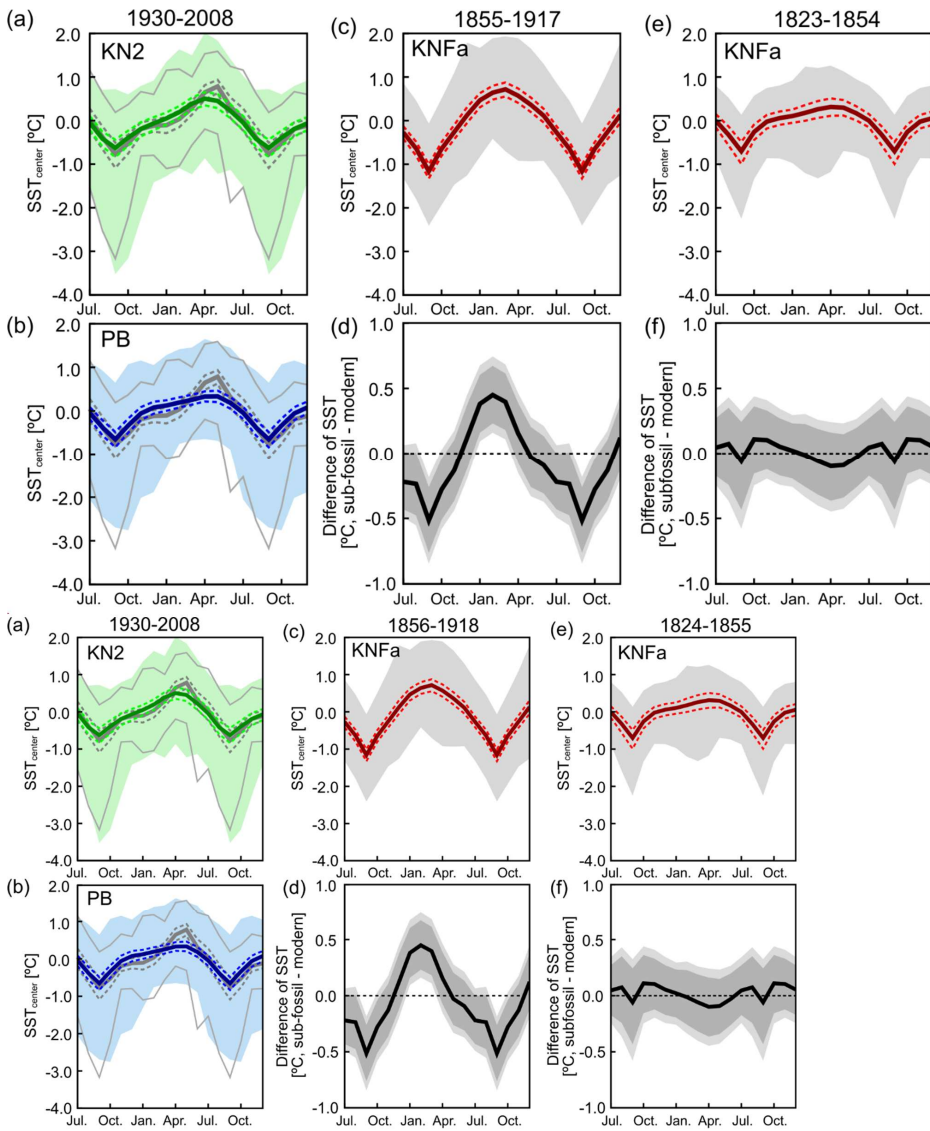
Figure 7: Mean seasonal cycles of SST_{center} derived from modern and sub-fossil Enggano corals. (a) 1930-2008, core KN2 (in green; solid line is monthly mean, dashed green lines are ±1σ, green shading indicates 99 % percentiles of monthly means). Satellite SST data (Huang et al., 2021) (mean removed, thick grey line is monthly mean, dashed grey lines are ±1σ; thin grey lines are 99 % percentiles of monthly means) are shown for comparison. (b) Same as (a), but for core PB (in blue; solid line is monthly mean, dashed blue lines are ±1σ, blue shading indicates 99 % percentiles of monthly means). (c) Same as (a) but for core KNFa in the time period from 1856̶5̶ ̶1̶9̶1̶7̶1918 (in red; solid line is monthly mean, dashed red lines are ±1σ, grey shading indicates 99 % percentiles of monthly means), (d) Difference of mean seasonal cycles: (1930-2008 monthly average data of KN2 and PB) minus (1856̶5̶ ̶1̶9̶1̶7̶1918 of monthly average data of KNFa), with 95 and 99 % confidence levels (dark and light shading, respectively) based on a 20 000 sample Monte Carlo. Note the inflated y-axis. (e) and (f) same as (c) and (d) for the time period from 1̶8̶2̶3̶1824-1855̶4̶ (KNFa).

16
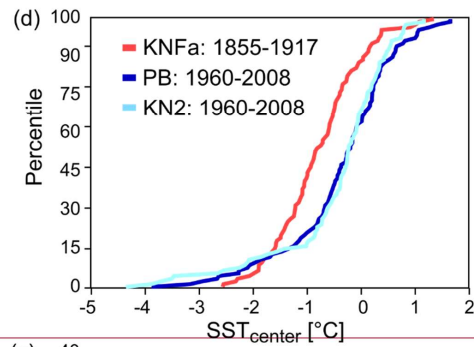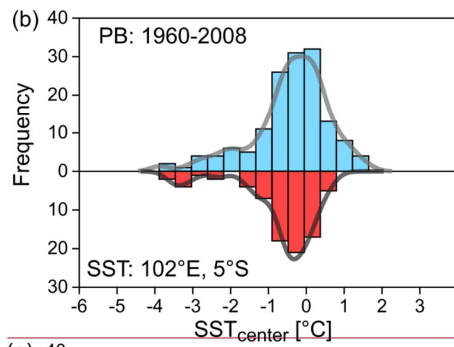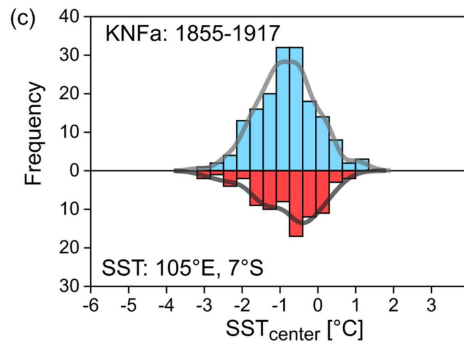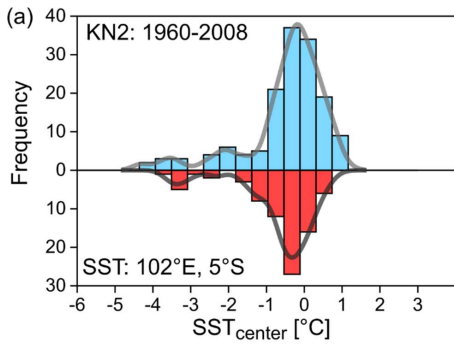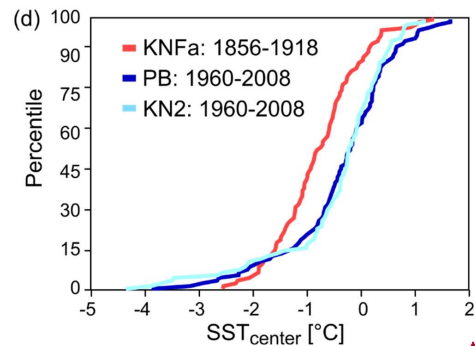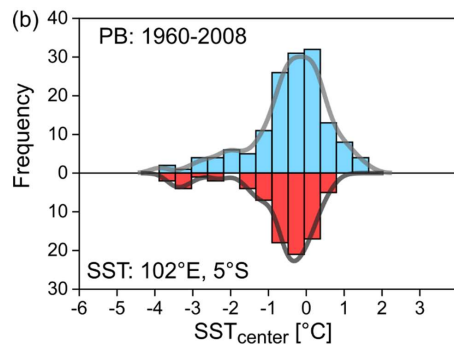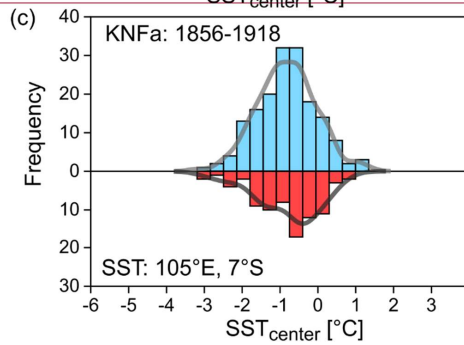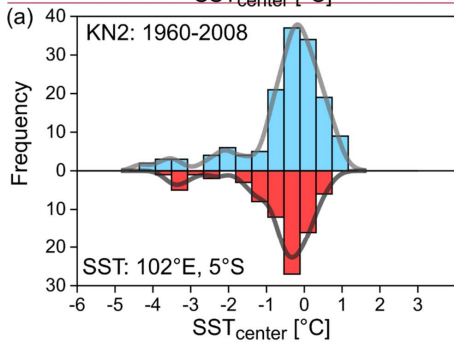
Figure 8: (a)-(c): Distribution of September-November monthly mean SST$_{centre}$ inferred from the Enggano Sr/Ca records (in blue) compared to satellite SSTs (in red, OI SST, ¼° grid, 1982-2008, centred to its mean) (Huang et al., 2021). Thick grey lines are the Kernel density functions of the histograms. (a, b) Modern September-November SST$_{centre}$ (KN2 and PB) from 1960-2008 shows the same distribution as SSTs in the grid centred at Enggano island. The negative skewness reflects the occurrence of extreme pIOD events. Between 1856~~5-1917~~1918, September-November SST$_{centre}$ (KNFa) shows a symmetric distribution, comparable to the SST distribution seen today at 7°S. (d) Percentiles of SST$_{centre}$ shown in (a), (b) and (c). See Table A3 and A4 for a comparison of the distributions using a Kolmogorov-Smirnov test. Histograms and percentiles were computed using PAST (Hammer et al., 2001).

5.4 Meridional and zonal Indian Ocean SST gradients in historical data

In this section, we assess how changes in the meridional and zonal SST gradients across the tropical Indian Ocean may have contributed to the change in mean climate inferred from the Enggano corals. We first confirm that the corals from Enggano Island track meridional changes in the North-South-temperature gradient in the eastern Indian Ocean using satellite data. Following Weller et al. (2014), the meridional temperature gradient is calculated as the difference between SST averaged over (90-110°E, 2.5-7.5°N) and (90-110°E, 10°S-Equator). This index correlates negatively with September-November SST at Enggano Island (satellite SST, 1982-2024) and coral SST$_{centre}$ in the period of overlap (1982-2008) (Fig. A10). The North-South SST gradient calculated from satellite SST correlates with the North-South temperature gradient calculated from HadCRUT5 (Morice et al., 2021), which extends back to historical periods with a resolution of 5 x 5° grids. HadCRUT5 blends SST and surface air temperatures, but does not use spatial interpolation to fill data gaps (Morice et al., 2021), providing the best coverage of actual historical temperature data. Note that the northern box of HadCRUT5 is averaged from the equator to 10°N due to the lower spatial resolution of the dataset, and slightly underestimates the magnitude of interannual variability (Fig. A10). Between 1930 and 2008, September-November SST$_{centre}$ inferred from the modern Enggano corals correlates negatively with the meridional temperature gradient calculated from HadCRUT5 (Fig. A10).

In the satellite era, interannual variations of meridional and zonal SST gradients across the tropical Indian Ocean are coupled, i.e. a northward contraction of the Indian Ocean Warm Pool is typically also associated with a reversal of the zonal SST gradient, resulting in a pIOD event (Weller and Cai, 2014). Only few strong IOD events, such as the event of 1982, feature large zonal anomalies while the southern boundary of the TCZ remains south of Enggano Island (Weller et al., 2014). To further assess this relationship on historical time scales, we have compared meridional and zonal temperature gradients across the tropical Indian Ocean using HadCRUT5 (Morice et al., 2021). Note, however, that these long-term temperature gradients may be affected by sparse observations in the Indian Ocean prior to the satellite era (Gopika et al., 2020). The zonal temperature gradient is calculated as the temperature difference between (50-70°E, 10°S-10°N) and (90-110°E, 10°S-Equator). The zonal gradient shows a long-term increase reflecting the continuous warming of the western Indian Ocean, which appears to have started before the beginning of historical records (Fig. 9) (Roxy et al., 2014; Gopika et al., 2020; Pfeiffer et al., 2017), at rates exceeding eastern Indian Ocean warming (Gopika et al., 2020). In contrast, the meridional temperature gradient calculated from HadCRUT5 does not show a significant long-term trend. It reverses in sign and diverges from the zonal SST gradient prior to 1925, with a warmer north-eastern Indian Ocean relative to the south-eastern tropical Indian Ocean (Fig. 9). In this period, the meridional SST gradient may have even exceeded present-day values. Taken together, this suggests a warmer eastern Indian Ocean (relative to the west) with a stronger north-south meridional temperature gradient in the east. Similar results (not shown) where obtained using GISS Surface Temperature data (GISTEMP v4, 250 km smoothing) (Lenssen et al., 2019). Thus, the positive linear relationship between meridional and zonal SST gradients seen in the satellite era (Weller and Cai, 2014) does not hold on historical periods. The positive north-south SST gradient prior to ~1930 should have driven stronger SE winds off Java and Sumatra in austral spring, which may have shifted the mean position of the southern boundary

18

of the TCZ to the north of Enggano Island in September-November, supporting our interpretation of the Enggano coral Sr/Ca data.

470 **Figure 9: Temperature gradients in the tropical Indian Ocean. North-South (red; 90-110°E, 0-10°N minus 90-110°E, 10°S-Equator) and West-East (blue; 50-70°E, 10°S-10°N minus 90-110°E, 10°S-Equator) Indian Ocean temperature gradients using HadCRUT5 (Morice et al., 2021). Temperature gradients shown are smoothed using 21 year moving averages. Pink and blue shades indicate uncertainty (1σ) calculated using bootstrap methods. The West-East Indian Ocean temperature gradient increases steadily since 1880 (p < 0.01, Mann-Kendall test), but possibly decelerates after 1939 (95%CI: 1876~1943 CE, SiZer test (Chaudhuri and Marron,**
475 **1999), blue horizontal line with circle). The exact onset of the deceleration cannot be determined (note the large 95% confidence levels of the SiZer test). The North-South Indian Ocean temperature gradient does not show a significant long-term trend (p > 0.1, Mann-Kendall test) and reverses prior to 1947 (95%CI 1940~1953 CE, red horizontal line with circle).**

5.5 Comparison with other proxy records from the SE tropical Indian Ocean

480 An annual mean warm pool SST reconstruction based on corals from various sites of the West Pacific Warm Pool and tree rings from Java extends back to the late 18th century (D'Arrigo et al., 2006). This reconstruction shows cooling prior the 1930s, which would be consistent with stronger SE trade winds and greater cooling seen at Enggano Island in austral spring. Warm intervals interrupted by short cold spells between 1815-1850 correspond to the section of 'modern' SST seasonality that is seen in the Enggano record between ~~1823~~1824 and 185~~5~~4.

485 The first coral reconstruction of coastal upwelling associated with the IOD derives from a coral δ^{18}O record from the northern Mentawai Islands, located approximately 4 ° further north of Enggano Island (Fig. 2, Fig. 3, Fig. A2, Fig. A3) (Abram et al., 2008). The record lies at the northern edge of the Sumatra upwelling zone and extends from 1858 to 1997 (Fig. 10), i.e. it overlaps with the two modern Enggano coral Sr/Ca records and the upper third of the sub-fossil coral KNFa. The northern
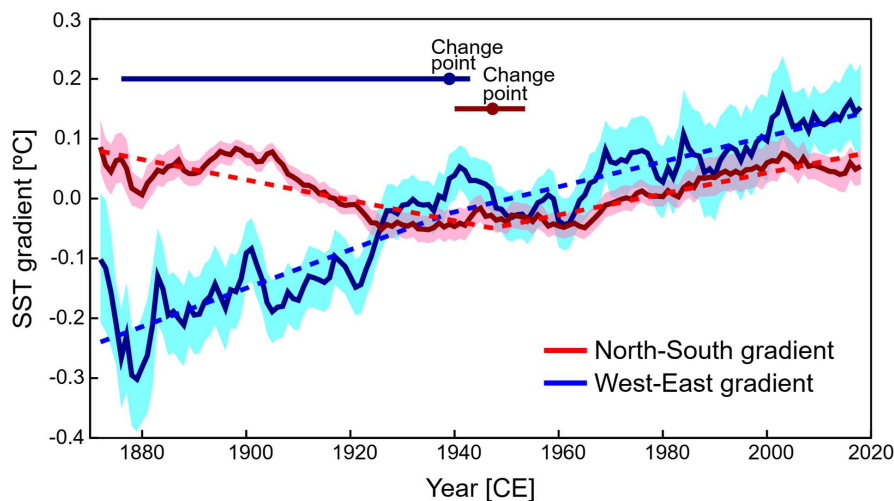
Mentawai coral records the most extreme pIOD events in 1961, 1994 and 1997, when the boundary of the TCZ shifted far
490 northwards, but not the events of 1963 and 1967 that are seen in the modern Enggano Sr/Ca records (Fig. 10). Wind-induced coastal upwelling did not extend that far north during these events (Abram et al., 2015). The northern Mentawai record thus provides constraints on the northward shift of the southern boundary of the TCZ in austral spring. The northern Mentawai record does not show the increase in SST seasonality between 185~~6~~5 and ~~1917~~1918 seen in the KNFa record (Fig. 10, Fig. A11), which is attributed to a strengthening of the SE winds off Java and Sumatra in austral spring driven by the Asian
495 monsoon. This would suggest that the boundary of the TCZ did not shift beyond the northern Mentawai Islands in this period. Prior to 1961, the northern Mentawai record shows one extreme pIOD event in 1877 that coincided with the very strong El Nino of 1877/78 (Abram et al., 2008). This event caused record drought and famine in much of Asia (Davis, 2002) and strong

19

warming in the western tropical Indian Ocean (Pfeiffer and Dullo, 2006; Charles et al., 1997). The Mentawai record thus suggests that one extreme pIOD event occurred between 1856~~5~~ and ~~1917~~1918 which was at least on par with the devastating event of 1997.

Note that we do not see an extreme cold spike that can be attributed to the 1877 event in the KNFa record. We attribute this to the frequent upwelling seen in this record in the 1856-1918 period. Modern SST data may serve as an analogue to understand this phenomenon: during extreme pIOD events, such as 1997, u~~p~~welling cools September-November SSTs to < 25 °C at all sites off the Java-Sumatra coast (Fig. A12). In other years, upwelling is spatially constrained to sites off Java, for example at 7 °S and 8 °S, where SSTs cool to ~24-25 °C in many years (Fig. A12). Th~~e cooling during~~ises ~~even~~ extreme ~~p~~IOD events like 1994, 1997, 2006 or 2019~~- is therefore much smaller relative to the mean September-November SSTs.~~ Between 1856~~5-1917~~1918, SST variability inferred from the~~the~~ KNFa record is comparable to the SST variability seen today off Java, at 7°S (Fig. 8, Table A4). This, combined with the age model uncertainty that derives from the~~-~~ U/Th ages (Fig. A7), makes it difficult to unequivocally identify the 1877 event in the KNFa record. It could be reflected in one of the larger cold spikes seen ~1880. Coral cores from various sites off the coast Sumatra can therefore help to constrain the occurrence and magnitude of historical IOD events that pre-date the instrumental record. The Mentawai record suggests that the 1877 pIOD event was comparable to the 1997 event, while the KNFa record from Enggano suggests that this event occurred in a mean climate with stronger SE monsoon winds and a northward shift of the TCZ. ~~Note that it would be much more difficult to identify this event at Enggano due to the increased upwelling there in every year.~~

A reconstruction of the Indian Ocean Dipole Mode Index using a network of coral oxygen isotope records from the tropical Indian Ocean comprising the northern Mentawai record, Bali (Charles et al., 2003) and the Seychelles (Pfeiffer and Dullo, 2006; Charles et al., 1997) suggests that two additional pIOD events occurred between 1856~~5~~ and ~~1917~~1918 (Abram et al., 2008; Abram et al., 2020). ~~Note, however, that T~~these events are not seen in the northern Mentawai record and may have been weaker than the 1877 event. Alternatively, they may have also be~~en~~ driven by warming in the western Indian Ocean, rather than cooling in the east (Jiang et al., 2022). Regardless of this, the low number of pIOD events between 1856~~5-1917~~1918 would support the interpretation that the Enggano Sr/Ca record shows a mean state change between 1856~~5-1917~~1918 in response to an enhanced meridional SST gradient in the eastern Indian Ocean, rather than an increase in IOD frequency. This de-coupling between meridional and zonal variability has no analogue in the reliable instrumental record. However, future projections also suggest that meridional and zonal variability may de-couple depending on the long-term evolution of the temperature gradients in the Indian Ocean (Weller et al., 2014).

New coral proxy data from South Pagai, which is part of the Southern Mentawai Islands and lies approximately halfway between the northern Mentawai Islands and Enggano, could help to further constrain the relationship between meridional and zonal variability in the Indian Ocean. South Pagai is likely the best candidate for a stationary IOD teleconnection (Abram et al., 2015). A modern coral δ^{18}O record from South Pagai extends back to 1959 and records all pIOD events seen in the modern Enggano Sr/Ca record (Pfeiffer et al., 2022). Unfortunately, there is no record from South Pagai that overlaps with the Enggano Sr/Ca data from 1856~~5-1917~~1918. A sub-fossil coral δ^{18}O record from South Pagai that extends from 1770-1820 shows 6 pIOD events in 50 years. This record pre-dates the ~~1823~~1824-1855~~4~~ section of the Enggano record, where seasonality again compares with the modern Enggano corals KN2 and PB.

Another independent source of information on low-frequency climatic changes in the SE tropical Indian Ocean is provided by sediment cores. Their temporal resolution and age control are much lower when compared to sub-fossil coral records, but their record is more continuous and covers longer time periods. Steinke et al. (2014a,b) investigated a sediment core in the Timor Sea, north-west of Sumba Island spanning the last 2000 years (Fig. 11). Sumba Island is located south-east of the main upwelling zone off the coast of Java (Fig. 2). In this region, moderate and extreme pIOD events cause anomalous cooling of SSTs (note that moderate pIODs tend to cause even stronger cooling than strong ones) (Fig. A3). A modern coral Sr/Ca record from nearby Timor Island (10 °S, 123 °E), which extends from 1914 to 2004 shows that decadal SST variability in this region

20

tracks decadal IOD variability (Cahyarini et al., 2014a). The top of the sediment core from Sumba Island is dated to 1984 ±6 years CE (Steinke et al., 2014a) (Fig. 11). The record includes mixed layer temperatures inferred from foraminiferal Mg/Ca ratios with a temporal resolution of ~5 years, and relative abundances of mixed layer and thermocline dwelling foraminifera with a temporal resolution of ~10 years (Fig. 11). Unfortunately, a turbidite limits the overlap with the Enggano Sr/Ca record

545   to 1845 ±9 years BP (Steinke et al., 2014a), which hampers a comparison with the shift back to modern SST seasonality between 1842 and 1854 seen in the coral record. Nevertheless, the sediment core data shows a cooling of SSTs from a mean of 25.0 °C between 1932-1984 to a mean of 23.8 °C between 1845 and 1928, i.e. the difference exceeds -1 °C, which is statistically significant based on a two-sided students t-test ($p<0.05$). The inferred decrease in mean SST is accompanied by an increase of thermocline dwelling foraminifera, while mixed-layer foraminifera abundance remained fairly constant (Fig.

550   11). This indicates that a shallowing of the thermocline in the SE tropical Indian Ocean prior to ~1930, favoring increased upwelling of cold water, was the most likely driver of the inferred cooling trend seen at Sumba Island. Steinke et al. (2014b) linked this decrease in mean SST and thermocline depth to stronger SE trade winds in the SE tropical Indian Ocean, which is fully consistent with our interpretation of the Enggano Sr/Ca record. Furthermore, (Steinke et al., 2014b) suggest that these changes are part of a longer-term trend to cooler temperatures and a shallower thermocline during the Little Ice Age, despite

555   some modulation by low-frequency variability. During the medieval warm period, SE Indian Ocean SSTs warmed again and the thermocline deepened, which should have reduced upwelling of cold water off Java and Sumatra (Steinke et al., 2014b). Interestingly, a 40-year sub-fossil coral Sr/Ca record from Lampung Bay, located between Java and Sumatra, suggests reduced seasonal and interannual (IOD) variability during the medieval warm period (Cahyarini et al., 2021), consistent with the record of Steinke et al. (2014b). Thus, the study of Steinke et al. (2014a,b) lends support to the changes in mean climate in the eastern

560   equatorial Indian Ocean inferred from the Enggano Sr/Ca record, and suggests that it may be part of a centennial trend that extends beyond the time period covered by the instrumental and coral SST record from the SE tropical Indian Ocean.
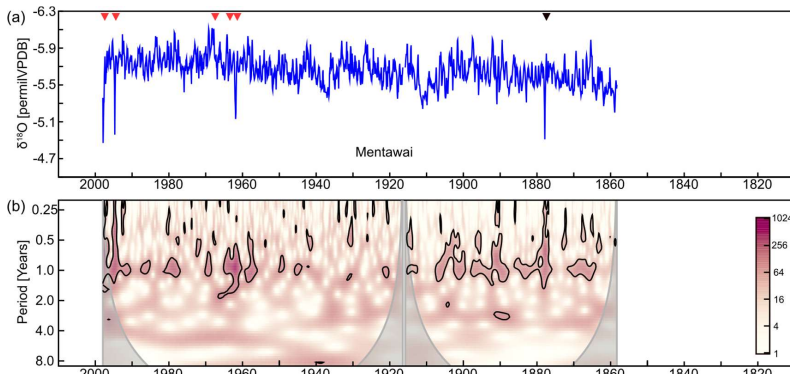
Figure 10: Monthly coral δ¹⁸O record from northern Mentawai from (Abram et al., 2008). (a) monthly mean coral δ¹⁸O (thin blue lines) and ten-year running averages (thick red line) from 1858-1997. Red arrows mark extreme pIOD events seen in the Sr/Ca

565   **record from Enggano (Pfeiffer et al., 2022). Note: The Mentawai coral record does not record the events of 1963 and 1967. One extreme pIOD event is recorded in 1877 (black arrow). (b) Wavelet Power spectrum of the Mentawai record, with largest variability on interannual periodicities. Wavelet Power spectrum was computed in R using the Morlet Wavelet. Thick black lines indicate significant periodicities at a certain time (p<0.05). Grey shading indicates cone of influence.**
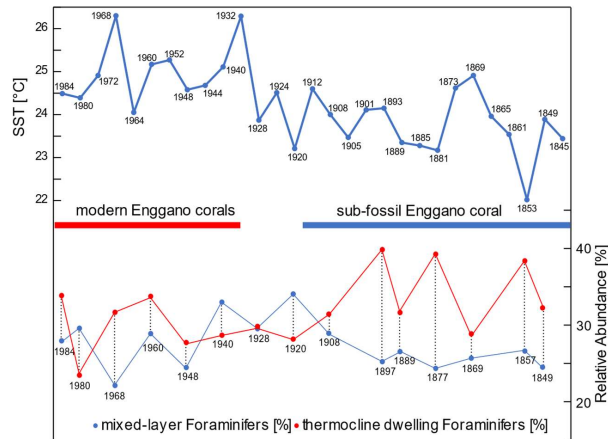
Figure 11. Top: Mean SSTs inferred from Foraminiferal Mg/Ca ratios from a sediment core taken off Sumba Island (Steinke et al., 2014a; Steinke et al., 2014b). Each dot represents one measurement, with estimated ages of (Steinke et al., 2014b). Red (blue) horizontal bars indicate time period covered by modern (sub-fossil) coral records from Enggano Island. Bottom: Relative abundance of mixed layer (blue dots) and thermocline dwelling (red dots) foraminifera (Steinke et al., 2014b). See text for discussion.

6 Summary and Conclusions

The Enggano Sr/Ca record reveals changes in SST seasonality in the SE tropical Indian Ocean on historical time scales. A period with enhanced seasonality occurs between 1856~~5~~ and ~~1917~~1918 due to a cooling of mean September-November SSTs. This indicates an early onset of the Asian summer monsoon coupled with a northward expansion and strengthening of the SE winds off Java and Sumatra, qualitatively consistent with low-frequency, centennial-scale changes inferred from high-resolution sediment core data (Steinke et al., 2014a,b). We attribute the enhanced seasonality to an enhanced meridional temperature gradient in the eastern tropical Indian Ocean, with warming in the north relative to the south, and a shift of the southern boundary of the TCZ to the north of 5°S in austral spring due to a stronger Asian summer monsoon. We note that the positive correlation between the meridional and the zonal SST gradient in the tropical Indian Ocean seen on interannual time scales does not hold on historical time periods. Between 1856~~5~~ and ~~1917~~1918, the magnitude of the mean September-November cooling at Enggano Island is comparable to the cooling seen today during 'weaker' extreme and moderate pIOD events. As even moderate IOD events may have significant climatic impacts in Indian Ocean rim countries, this warrants further investigation, especially since our data indicate quite abrupt transitions in seasonality on historical time periods. We conclude that meridional variability in the SE tropical Indian Ocean needs to be better understood. An array approach combining coral proxy data and high-resolution sediment core records along the coasts of Java and Sumatra would be ideal to better capture the full spectrum of climate variability in the SE tropical Indian Ocean.

Appendices

Table A1: Coral growth rates

Coral core	Growth rate (mm/year)	Standard deviation (1σ)
PB	14.3	3.6
KN2	10.3	2.5
KNFa (1865-19187)	10.8	2.4
KNFa (18231824-18554)	11.4	2.2

Table A2. Uranium and thorium isotopic compositions and ages of coral core KNFa by MC-ICPMS, Thermo Electron Neptune, at the National Taiwan University. Table A2: Uranium and Thorium isotopic compositions and ^{230}Th ages of core KNFa by MC-ICPMS, Thermo Electron Neptune, at National Taiwan University.

Sample ID	Weight g	^{238}U ppb^a	^{232}Th ppt	d^{234}U measured^d	$[^{230}Th/^{238}U]$ activity^c	$[^{230}Th/^{232}Th]$ ppm^d	Age uncorrected	Age corrected^{c,e}	d^{234}U$_{initial}$ corrected^b	AD uncorrected	AD corrected
KNFa(2/11)	0.1785	1870.4 ±2.0	2115.3 ±5.7	146.2 ±1.8	0.001395 ±0.000030	20.33 ±0.44	132.8 ±2.9	107 ±13	146.2 ±1.8	1,881 ±3	1,907 ±13
KNFa(3/11)*	0.2028	2553.4 ±2.1	494.8 ±2.4	143.2 ±1.3	0.001241 ±0.000013	105.6 ±1.2	118.4 ±1.3	113.9 ±2.6	143.2 ±1.3	1,897.1 ±1.3	1,901.6 ±2.6
KNFa(5/11)*	0.1815	1845.4 ±1.7	521.5 ±2.7	143.1 ±1.8	0.001621 ±0.000015	94.6 ±1.0	154.7 ±1.4	148.2 ±3.6	143.2 ±1.8	1,859.0 ±1.4	1,865.5 ±3.6
KNFa(7/11)*	0.2011	2565.9 ±2.1	330.6 ±2.3	143.8 ±1.2	0.001713 ±0.000013	219.2 ±2.2	163.4 ±1.2	160.4 ±1.9	143.8 ±1.2	1,852.1 ±1.2	1,855.1 ±1.9
KNFa(8/11)	0.2092	1842.3 ±2.2	224.9 ±2.2	144.9 ±1.6	0.001658 ±0.000011	223.9 ±2.7	158.0 ±1.1	155.2 ±1.8	144.9 ±1.6	1,855.7 ±1.1	1,858.5 ±1.8
KNFa(10/11)	0.1965	1791.0 ±2.0	260.4 ±2.4	145.7 ±1.7	0.001923 ±0.000014	218.2 ±2.6	183.2 ±1.4	179.9 ±2.2	145.7 ±1.7	1,830.5 ±1.4	1,833.8 ±2.2

Sample ID	Weight g	^{238}U 10^{-9}g/g^a	^{232}Th 10^{-12}g/g	δ^{234}U measured^d	$[^{230}Th/^{238}U]$ activity^c	$[^{230}Th/^{232}Th]$ atomic (x 10^{-5})	Age uncorrected	Age corrected^{c,d}	Age AD	δ^{234}U$_{initial}$ corrected^b
KNFa(2/11)$^{\#}$	0.1785	1870.4 ± 2.0	2115.3 ± 5.7	146.2 ± 1.8	0.001395 ± 0.000030	20.33 ± 0.44	132.8 ± 2.9	105 ± 17	1909.049 ± 17	146.2 ± 1.8
KNFa(3/11)$^{\#}$	0.2028	2553.4 ± 2.1	494.8 ± 2.4	143.2 ± 1.3	0.001241 ± 0.000013	105.6 ± 1.2	118.4 ± 1.3	113.4 ± 3.2	1902.1391 ± 3.2	143.2 ± 1.3
KNFa(5/11)$^{\#}$	0.1815	1845.4 ± 1.7	521.5 ± 2.7	143.1 ± 1.8	0.001621 ± 0.000015	94.6 ± 1.0	154.7 ± 1.4	147.7 ± 4.3	1866.0439 ± 4.3	143.2 ± 1.8
KNFa(7/11)$^{\#}$	0.2092	1842.3 ± 2.2	224.9 ± 2.2	144.9 ± 1.6	0.001658 ± 0.000011	223.9 ± 2.7	158.0 ± 1.1	155.0 ± 2.1	1858.7405 ± 2.1	144.9 ± 1.6
KNFa(9/11)$^{\#}$	0.2011	2565.9 ± 2.1	330.6 ± 2.3	143.8 ± 1.2	0.001713 ± 0.000013	219.2 ± 2.2	163.4 ± 1.2	160.1 ± 2.2	1855.4426 ± 2.2	143.8 ± 1.2
KNFa(10/11)$^{\#}$	0.1965	1791.0 ± 2.0	260.4 ± 2.4	145.7 ± 1.7	0.001923 ± 0.000014	218.2 ± 2.6	183.2 ± 1.4	179.6 ± 2.5	1834.1338 ± 2.5	145.7 ± 1.7

$^{\#}$Chemistry was performed on September15th, 2013; *Chemistry on July 2nd, 2015.

Analytical errors are 2σ of the mean.

$^a[^{238}U] = [^{235}U]$ x 137.77 (±0.11‰) for marine samples (Hiess et al., 2012); $\delta^{234}U = ([^{234}U/^{238}U]_{activity} - 1)$ x 1000.

$^b\delta^{234}U_{initial}$ corrected was calculated based on ^{230}Th age (T), i.e., $\delta^{234}U_{initial} = \delta^{234}U_{measured} X e^{\lambda 234*T}$, and T is corrected age.

$^c[^{230}Th/^{238}U]_{activity} = 1 - e^{-\lambda_{230}T} + (\delta^{234}U_{measured}/1000)[\lambda_{230}/(\lambda_{230} - \lambda_{234})](1 - e^{-(\lambda_{230} - \lambda_{234})T})$, where T is the age.

Decay constants used for age calculation are available in (Cheng et al., 2013).

^{d}Age corrections for samples were calculated using an estimated atomic $^{230}Th/^{232}Th$ ratio of 4.3 ± 2.5 x 10^{-6} (Chiang et al., 2023).

Chemistry was performed on Sep.15th, 2013
*Chemistry was performed on Jul. 2nd, 2015

Analytical errors are 2σ of the mean

$^a[^{238}U] = [^{235}U]$ x 137.77 (±0.11‰) for marine samples (Hiess et al., 2012); $\delta^{234}U = ([^{234}U/^{238}U]_{activity} - 1)$ x 1000

$^b\delta^{234}U_{initial}$ corrected was calculated based on ^{230}Th age (T), i.e., $\delta^{234}U_{initial} = \delta^{234}U_{measured} X e^{\lambda 234*T}$, and T is corrected age.

$^c[^{230}Th/^{238}U]_{activity} = 1 - e^{-\lambda_{230}T} + (\delta^{234}U_{measured}/1000)[\lambda_{230}/(\lambda_{230} - \lambda_{234})](1 - e^{-(\lambda_{230} - \lambda_{234})T})$, where T is the age.

Decay constants are 9.1705 x 10^{-6} yr^{-1} for ^{230}Th, 2.8221 x 10^{-6} yr^{-1} for ^{234}U (Cheng et al., 2012), and 1.55125 x 10^{-10} yr^{-1} for ^{238}U (Jaffey et al., 1971)

^{d}The degree of detrital ^{230}Th contamination is indicated by the $[^{230}Th/^{232}Th]$ atomic ratio instead of the activity ratio.

^{e}Age corrections for samples were calculated using an estimated atomic $^{230}Th/^{232}Th$ ratio of 4 ± 2 ppm (Shen et al., 2008).

Table A3: Results of Kolmogorov-Smirnov test (two samples) comparing the distributions of monthly September, October and November coral Sr/Ca data. D: distance between the empirical distribution functions. The null hypothesis that the samples are drawn from the same distribution is rejected if p<0.01 (bold numbers).

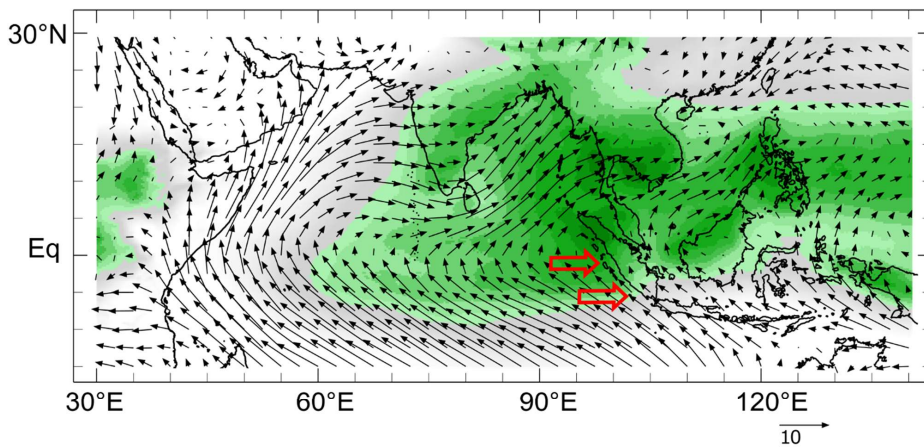| coral	PB	KN2	KNFa (18~~65~~-~~1917~~1918)
PB	x	D: 0.075	D: 0.3
KN2	p: 0.80	x	D: 0.36
KNFa (18~~65~~-~~1917~~1918)	**p: 0.001**	**p: 0.001**	x

Table A4: Results of Kolmogorov-Smirnov test (two samples) comparing the distributions of monthly September, October and November satellite SSTs from 1982-2008 at 5°S and 7°S (centered) with SST$_{centred}$ inferred from the corals. The null hypothesis that the samples are drawn from the same distribution is rejected if p<0.01 (bold numbers).

	PB	KN2	KNFa (18~~65~~-~~1917~~1918)
SST 102°E,5°S	p: 0.066	p: 0.127	**p: 0.001**
SST 105°E,7°S	**p: 0.005**	**p: 0.001**	p: 0.0358

655

25

(a) Mean September OLR and surface winds, 1991-2023

### (b) Mean September OLR and surface winds during extreme pIOD events
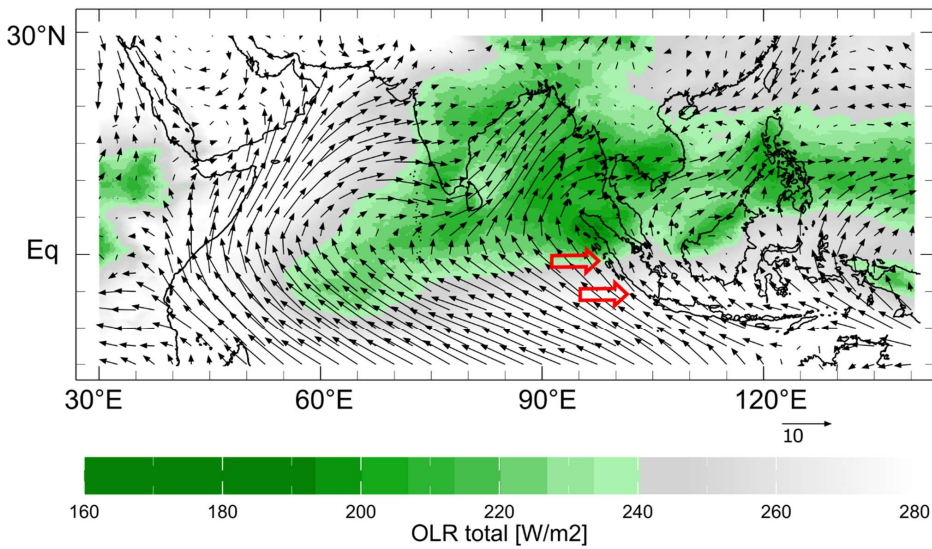
Figure A2: Evolution of coastal upwelling off Java and Sumatra in austral spring (June-November) as expressed in the standard deviation of monthly mean SST (colors). Coastal upwelling starts off Java in June, strengthens in July and spreads to southern Sumatra in July/August. In September/October, upwelling reaches the Mentawai islands located between 3° S and the equator. Coastal upwelling subsides in November. Arrows mark position of Enggano (E) and Mentawai (M). Charts were computed at the knmi climate explorer (https://climexp.knmi.nl)
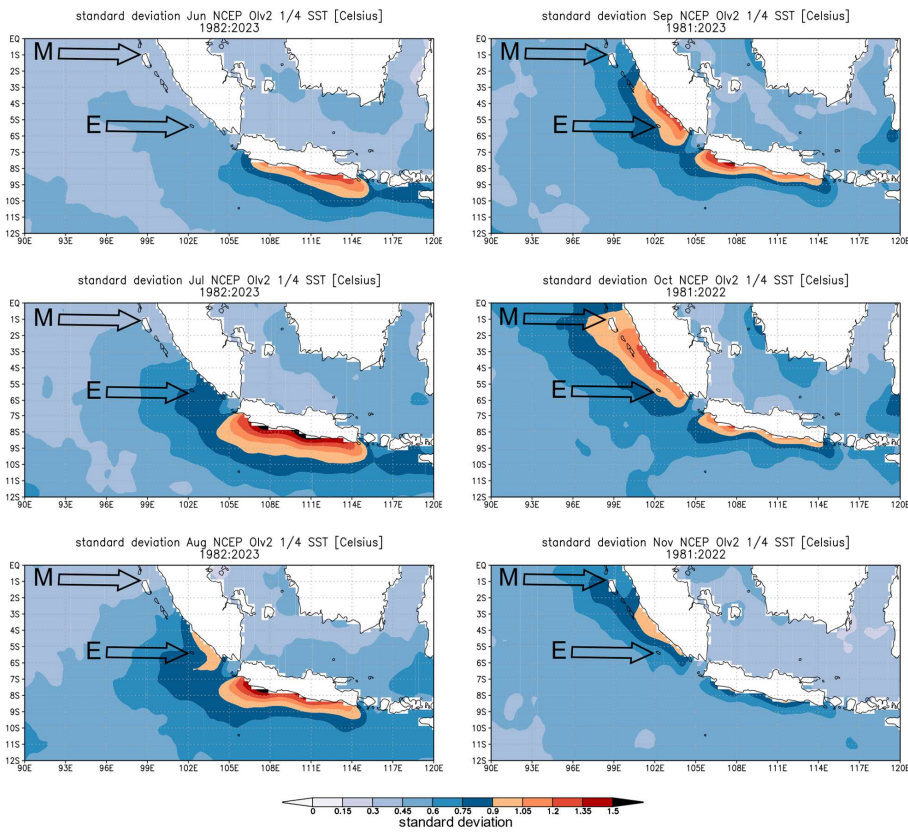
Figure A3: Composite maps of September-November SST anomalies during (a) extreme pIOD events (1994, 1997, 2006, 2019) and (b) moderate pIOD events (1982, 1983, 2012, 2015). Arrows mark position of Enggano (E), Mentawai (M) and Sumba (S). Thick black lines mark zero contours, thin solid lines positive anomalies and thin dashed lines negative anomalies at 0.5° C steps. Data from AVHRR-OI SST (1/4° grids, 1982-2022) (Huang et al., 2021). Charts computed at https://iridl.ldeo.columbia.edu/.
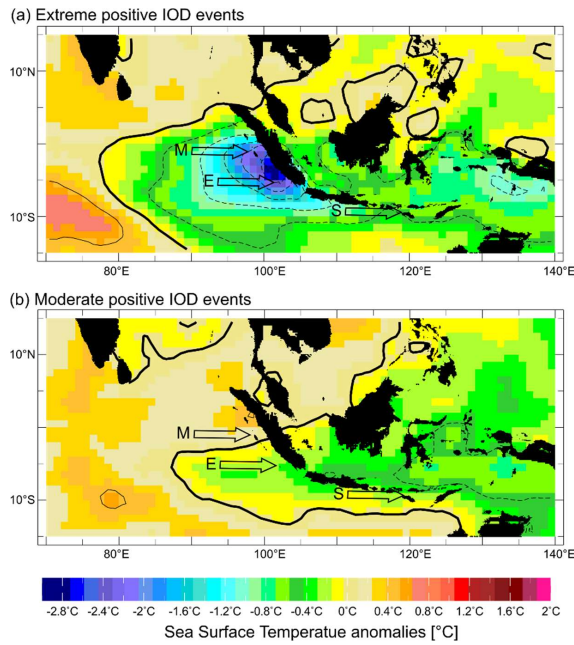
Figure A4: Luminescence scan of the sub-fossil coral core KNFa from Enggano. Core slabs are numbered. Note the dull, mottled appearance of the core top, which extends to the top of slab 2 and indicates potential secondary alteration. Parts of slab 6 look similar, although the effect is not as pronounced. These parts and adjacent transects were investigated using the Hitachi SU3900 Scanning electron microscope (SEM) with extra-large chamber. Slab 10 and 11 show localized alterations which occur in areas affected by bioerosion.

28
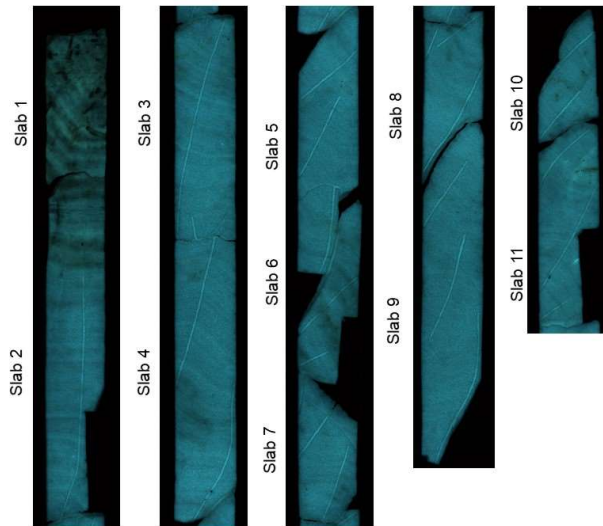
Figure A5: Hitachi SU3900 Scanning electron microscope with extra-large chamber. The sample holder has a diameter of 28 cm, shown here with slab 6 of core KNFa.
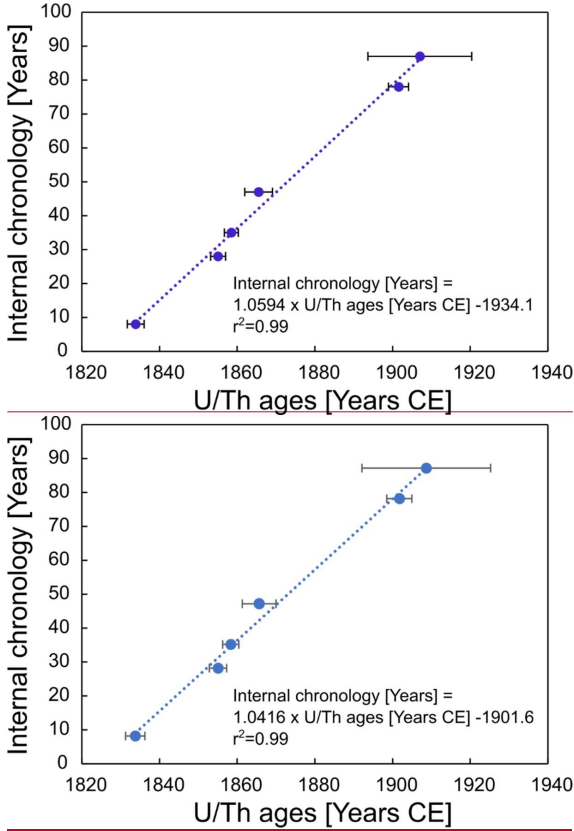

Figure A6: Scanning electron microscopy images showing pristine and diagenetic altered parts of sub-fossil coral KNFa. The top 14 cm of the core shows several macroscopic bioerosion traces on x-ray images (Fig. 4). This interval (a and b) is characterized by filamentous microborings (MB), dissolution (D) of centers of calcification and secondary aragonite (SA) cement. The degree of cementation is variable, ranging from (a) pristine coral skeletons and traces of cement to (b) more pervasive fibrous aragonite cement (5 to 10 μm-length). The interval below 14 cm is generally pristine (c) showing smooth primary aragonite (PA) skeletal surfaces. The only exception occurs in an interval from the base of slab 5 to the top of slab 7 (Fig. 5). A patch of secondary aragonite cement on transect 10 of slab 6 caused an extreme spike in the proxy record with unusually low Sr/Ca ratio of 9.32 mmol/mol. This 'false alarm' spike escaped detection by our first standard diagenetic screening, but was identified by our semi contentious SEM screening along the proxy sampling track.
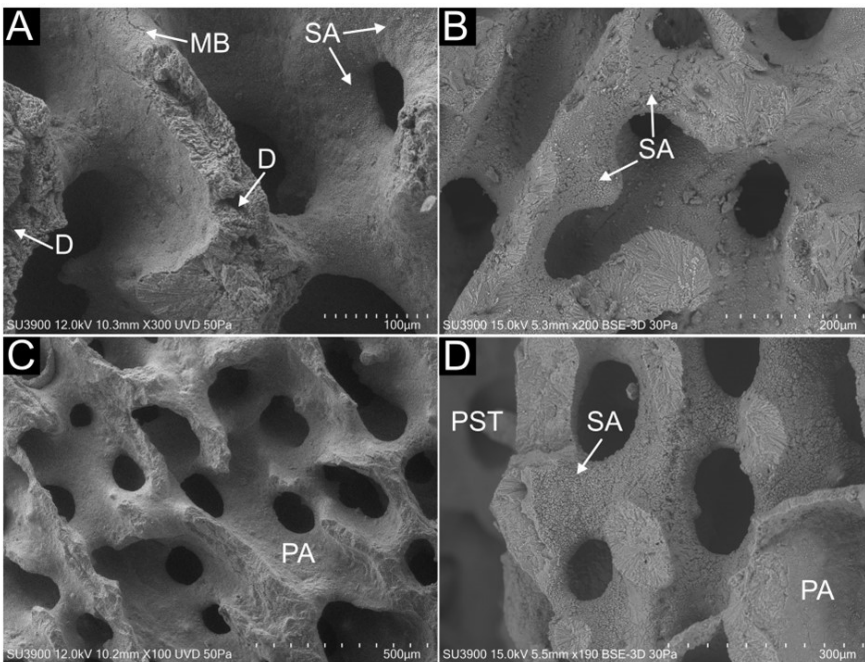
Figure A7: Corrected U/Th ages of core KNFa with 2σ uncertainties vs. the number of years estimated from seasonal cycles in coral Sr/Ca. The oldest year of KNFa is year 1. The age of the coral core was estimated from the intercept of the linear regression between the U/Th ages and the annual cycles of Sr/Ca (Fig. 5), assuming that the slope of this regression is one (i.e. assuming that the U/Th ages agree with the number of annual cycles seen in coral Sr/Ca) (Domínguez-Villar et al., 2012). The base of KNFa is dated to 1824~~3~~ ± ~~32.~~4 (2σ) years CE. The floating age uncertainty was estimated with a Monte Carlo approach (20,000 loops) using the 2σ U/Th error.

Internal chronology [Years] =
1.0594 x U/Th ages [Years CE] -1934.1
r^2=0.99

Internal chronology [Years] =
1.0416 x U/Th ages [Years CE] -1901.6
r^2=0.99

Figure A8: Violin and boxplots showing the distribution of monthly mean SSTs inferred from the modern Enggano corals (PB, KN2) compared with satellite SST (OI SST, ¼° grid) from 2008-1982 (Huang et al., 2021). Coral Sr/Ca has been centered to its mean and converted to SST assuming a Sr/Ca-SST relationship of -0.06 mmol mol^{-1} 1 °C^{-1}. Open circles (stars) indicate outliers exceeding ±1 (±1.5) standard deviations of the interquartile range. Violin plots computed using PAST (Hammer et al., 2001).
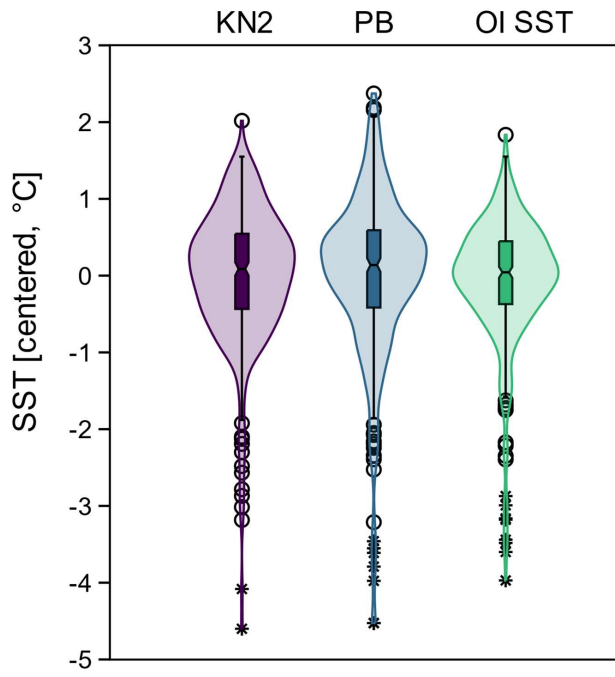
Figure A9: Modern and sub-fossil, monthly interpolated coral Sr/Ca time series from Enggano. (a) The complete Enggano Sr/Ca record comprises two modern (PB, KN2) and one sub-fossil core (KNFa) and extends from 1930-2008, ~~1869~~1869-~~1917~~1918 and ~~1823~~1824-~~1861~~1862. Thin blue and green lines are monthly data, thick red solid and dashed lines are 10-year running means. Note

that the sub-fossil record has a floating chronology based on U/Th dating with an age uncertainty of ± ~~3~~2.~~4~~ years (2σ). Relative changes in Sr/Ca reflect temperature variations with a mean Sr/Ca-SST relationship of -0.06 mmol mol 1 °C[-1] (Watanabe and Pfeiffer, 2022), which corresponds to one tick mark on the y-axis. Positive Sr/Ca anomalies in 2006,1997,1994, 1967, 1963 and 1961 indicate extreme pIOD events (red arrows). The sub-fossil record from KNFa indicates an extreme pIOD event in ~~~1825~~1826 (black arrow). Events in 190~~8~~7 and 191~~7~~6 may be comparable with the comparatively weaker, but still extreme pIOD of 2006. (b) and (c)

distribution of monthly coral Sr/Ca data in ~20-year bins shown as violin and boxplots. Values >1 standard deviation (>1.5 standard deviations) above or below the 1.5 % interquartile range are plotted as open circles (stars). Outliers reflect extreme pIOD events. (b) Cores PB and KN2, 1930-2008. The Sr/Ca distributions are negatively skewed in 1990-2008- and 1950-1969- due to the occurrence of extreme pIOD events. Note the consistent shift in the medians of PB and KN2 Sr/Ca data, indicating that vital effects remained stable over time. (c) Data from KNFa shows a symmetric distribution between ~185~~1~~5-~~1917~~1918, with a larger spread around the

median and few outliers. Between 189~~2~~43 and 185~~0~~54, the Sr/Ca distribution is comparable to modern values. Violin plots computed using PAST (Hammer et al., 2001).

32
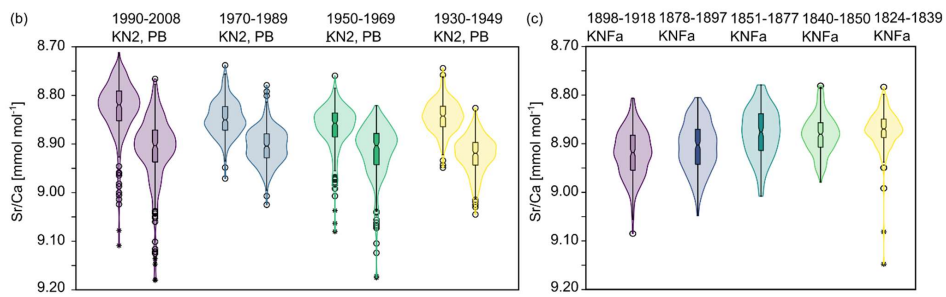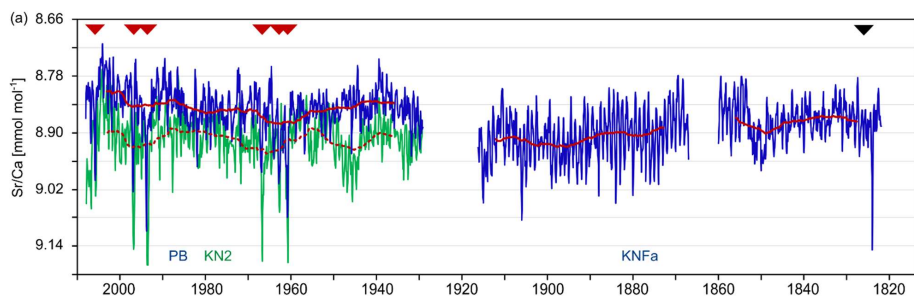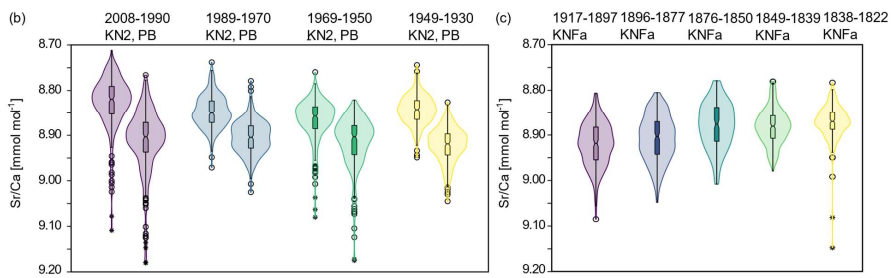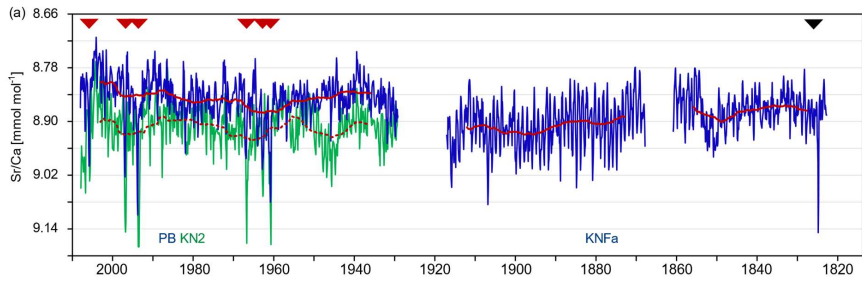
745 **Figure A10: North-South temperature gradient in the tropical Indian Ocean from 1930-2023 and September-November SST at Enggano. (a) and (b) North-South temperature gradient in the eastern Indian Ocean calculated from satellite SST (AVHRR SST, ¼° grid, available since 1982) (Huang et al., 2021) compared with HadCRUT5 temperatures (Morice et al., 2021). (c) Mean September-November SST at Enggano (AVHRR) and SST$_{centre}$ inferred from KN2 and PB compared with the North-South SST gradient calculated from AVHRR. (d-f) Linear regression of September-November SST (AVHRR) at Enggano, SST$_{centre}$ from KN2**
750 **(e) and PB (d) with the North-South SST gradient (AVHRR). (g) Same as (c) using the HadCRUT5 North-South temperature gradient. SST at Enggano correlates negatively with the meridional temperature gradient (colder SSTs at Enggano correspond to a stronger meridional gradient).**
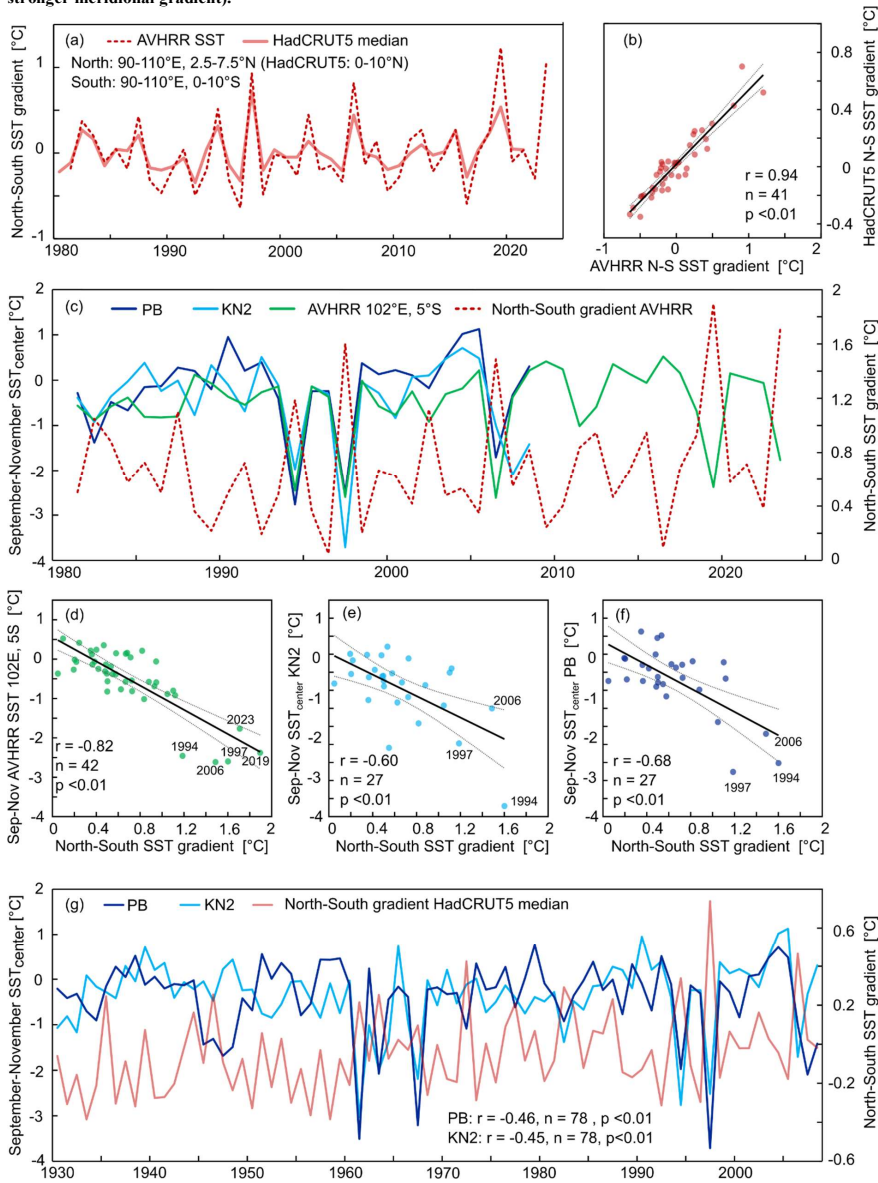
755 **Figure A11: Mean seasonal cycle of SST inferred from the from Mentawai coral δ¹⁸O record (Abram et al., 2008). Left: 1918-1997, Middle: 1860 (end of record) ~~1917~~1918. Right panel: the difference between the mean seasonal cycles (thick black line) in (a) and (b) is not significant. 95% (dark grey) and 99% confidence levels (light grey) overlap with the zero line. Significance was assessed with Monte Carlo as in Pfeiffer et al., 2022.**

760
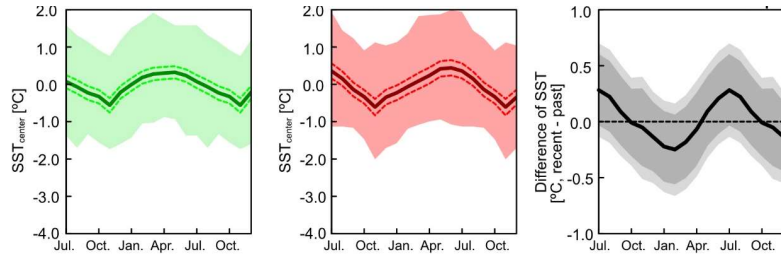
Figure A12: Magnitude of seasonal cooling compared with IOD-induced upwelling along the coast of Java and Sumatra. (a) The standard deviation of September-November SST indicates areas of coastal upwelling off the coast of Java and Sumatra. (b) The skewness of September-November SSTs reflects coastal upwelling associated with pIOD events**, which reaches Sumatra. Arrows in**
765 **(a) and (b) mark location of Enggano Island (E) and northern Mentawai Island (M). Charts were computed at the knmi climate explorer (https://climexp.knmi.nl). (c) Monthly mean satellite SST (OI SST, ¼° grid) from 1982-2024 (Huang et al., 2021) off the coasts of Java and Sumatra. S~~a~~ymbols indicate centers of SST grids in (a) and (b). Coastal upwelling cools SSTs to < 24°-25°C at all sites, resulting in uniformly cool SSTs during extreme positive IOD events (red arrows) when upwelling reaches the northern Mentawai Islands, for example in 1997. In other years, coastal upwelling and cooling is spatially restricted to sites south of 7°S,**
770 **making it harder to identify extreme pIOD events there. The intensity of pIOD events therefore mainly impacts/is seen in the northward extend of the cold anomalies off Sumatra.**

(a) Standard deviation, Sep-Nov OI SST [°C], 1982-2022   (b) Skewness, Sep-Nov OI SST [°C], 1982-2022

(c) Monthly mean OI SST [°C], 1982-2022, Java to Sumatra

35
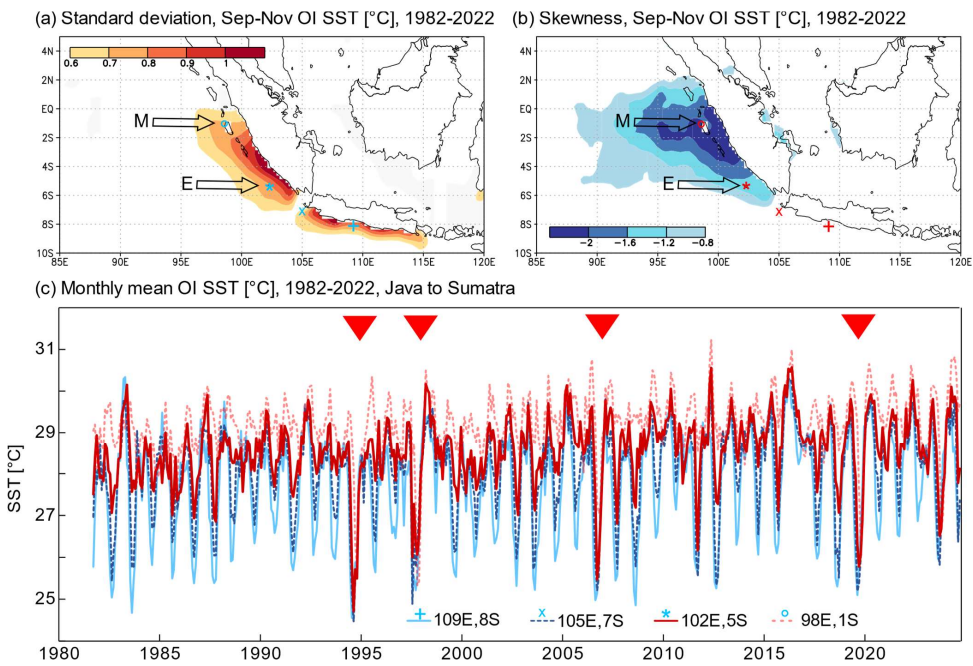
775   References

Abram, N. J., Dixon, B. C., Rosevear, M. G., Plunkett, B., Gagan, M. K., Hantoro, W. S., and Phipps, S. J.: Optimized coral
       reconstructions of the Indian Ocean Dipole: An assessment of location and length considerations, Paleoceanography, 30,
       1391–1405, doi:10.1002/2015PA002810, 2015.

Abram, N. J., Gagan, M. K., Cole, J. E., Hantoro, W. S., and Mudelsee, M.: Recent intensification of tropical climate
780   variability in the Indian Ocean, Nat. Geosci., 1, 849–853, doi:10.1038/ngeo357, 2008.

Abram, N. J., Gagan, M. K., Liu, Z., Hantoro, W. S., McCulloch, M. T., and Suwargadi, B. W.: Seasonal characteristics of
       the Indian Ocean Dipole during the Holocene epoch, Nature, 445, 299–302, doi:10.1038/nature05477, 2007.

Abram, N. J., Gagan, M. K., McCulloch, M. T., Chappell, J., and Hantoro, W. S.: Coral reef death during the 1997 Indian
       Ocean Dipole linked to Indonesian wildfires, Science (New York, N.Y.), 301, 952–955, doi:10.1126/science.1083841,
785   2003.

Abram, N. J., Wright, N. M., Ellis, B., Dixon, B. C., Wurtzel, J. B., England, M. H., Ummenhofer, C. C., Philibosian, B.,
       Cahyarini, S. Y., Yu, T.-L., Shen, C.-C., Cheng, H., Edwards, R. L., and Heslop, D.: Coupling of Indo-Pacific climate
       variability over the last millennium, Nature, 579, 385–392, doi:10.1038/s41586-020-2084-4, 2020.

Allison, N., Finch, A. A., Webster, J. M., and Clague, D. A.: Palaeoenvironmental records from fossil corals: The effects of
790   submarine diagenesis on temperature and climate estimates, Geochimica et Cosmochimica Acta, 71, 4693–4703,
       doi:10.1016/j.gca.2007.07.026, 2007.

Ashok, K., Guan, Z., and Yamagata, T.: Influence of the Indian Ocean Dipole on the Australian winter rainfall, Geophysical
       Research Letters, 30, doi:10.1029/2003GL017926, 2003.

Behera, S. K., Luo, J.-J., Masson, S., Delecluse, P., Gualdi, S., Navarra, A., and Yamagata, T.: Paramount Impact of the
795   Indian Ocean Dipole on the East African Short Rains: A CGCM Study, J. Climate, 18, 4514–4530,
       doi:10.1175/JCLI3541.1, 2005.

Cahyarini, S. Y., Pfeiffer, M., Dullo, W.-C., Zinke, J., Hetzinger, S., Kasper, S., Grove, C., and Garbe-Schönberg, D.:
       Comment on "A snapshot of climate variability at Tahiti at 9.5 ka using a fossil coral from IODP Expedition 310" by
       Kristine L. DeLong, Terrence M. Quinn, Chuan-Chou Shen, and Ke Lin, Geochem. Geophys. Geosyst., 12, n/a-n/a,
800   doi:10.1029/2010GC003377, 2011.

Cahyarini, S. Y., Pfeiffer, M., Nurhati, I. S., Aldrian, E., Dullo, W.-C., and Hetzinger, S.: Twentieth century sea surface
       temperature and salinity variations at Timor inferred from paired coral δ 18 O and Sr/Ca measurements, Journal of
       Geophysical Research: Oceans, 119, 4593–4604, doi:10.1002/2013jc009594, 2014a.

Cahyarini, S. Y., Pfeiffer, M., Nurhati, I. S., Aldrian, E., Dullo, W.-C., and Hetzinger, S.: Twentieth century sea surface
805   temperature and salinity variations at Timor inferred from paired coral δ 18 O and Sr/Ca measurements, J. Geophys.
       Res. Oceans, 119, 4593–4604, doi:10.1002/2013JC009594, 2014b.

Cahyarini, S. Y., Pfeiffer, M., Reuning, L., Liebetrau, V., Dullo, W.-C., Takayanagi, H., Anwar, I. P., Utami, D. A., Garbe-
       Schönberg, D., Hendrizan, M., and Eisenhauer, A.: Modern and sub-fossil corals suggest reduced temperature variability
       in the eastern pole of the Indian Ocean Dipole during the medieval climate anomaly, Scientific reports, 11, 14952,
810   doi:10.1038/s41598-021-94465-1, 2021.

Cai, W., Zheng, X.-T., Weller, E., Collins, M., Cowan, T., Lengaigne, M., Yu, W., and Yamagata, T.: Projected response of
       the Indian Ocean Dipole to greenhouse warming, Nat. Geosci., 6, 999–1007, doi:10.1038/ngeo2009, 2013.

Charles, C. D., Cobb, K., Moore, M. D., and Fairbanks, R. G.: Monsoon–tropical ocean interaction in a network of coral
       records spanning the 20th century, Marine Geology, 201, 207–222, doi:10.1016/S0025-3227(03)00217-2, 2003.

815   Charles, C. D., Hunter, D. E., and Fairbanks, R. G.: Interaction Between the ENSO and the Asian Monsoon in a Coral
       Record of Tropical Climate, Science (New York, N.Y.), 277, 925–928, doi:10.1126/science.277.5328.925, 1997.

36

Chaudhuri, P. and Marron, J. S.: SiZer for Exploration of Structures in Curves, Journal of the American Statistical Association, 94, 807–823, doi:10.1080/01621459.1999.10474186, 1999.

Cheng, H., Lawrence Edwards, R., Shen, C.-C., Polyak, V. J., Asmerom, Y., Woodhead, J., Hellstrom, J., Wang, Y., Kong, X., Spötl, C., Wang, X., and Calvin Alexander, E.: Improvements in 230Th dating, 230Th and 234U half-life values, and U–Th isotopic measurements by multi-collector inductively coupled plasma mass spectrometry, Earth and Planetary Science Letters, 371-372, 82–91, doi:10.1016/j.epsl.2013.04.006, 2013.

Chiang, H.-W., Philibosian, B., Meltzner, A. J., Wu, C.-C., Shen, C.-C., Edwards, R. L., Chuang, C.-K., Suwargadi, B. W., and Natawidjaja, D. H.: Investigating spatio-temporal variability of initial 230Th/232Th in intertidal corals, Quaternary Science Reviews, 307, 108005, doi:10.1016/j.quascirev.2023.108005, 2023.

Cobb, K. M., Westphal, N., Sayani, H. R., Watson, J. T., Di Lorenzo, E., Cheng, H., Edwards, R. L., and Charles, C. D.: Highly variable El Niño-Southern Oscillation throughout the Holocene, Science ~~(New York, N.Y.)~~, 339, 67–70, doi:10.1126/science.1228246, 2013.

Corrège, T.: Sea surface temperature and salinity reconstruction from coral geochemical tracers, Palaeogeography, Palaeoclimatology, Palaeoecology, 232, 408–428, doi:10.1016/j.palaeo.2005.10.014, 2006.

D'Arrigo, R., Wilson, R., Palmer, J., Krusic, P., Curtis, A., Sakulich, J., Bijaksana, S., Zulaikah, S., La Ngkoimani, O., and Tudhope, A.: The reconstructed Indonesian warm pool sea surface temperatures from tree rings and corals: Linkages to Asian monsoon drought and El Niño–Southern Oscillation, Paleoceanography, 21, doi:10.1029/2005PA001256, 2006.

Davis, M.: Late Victorian holocausts: El Niño famines and the making of the third world, ACLS Humanities E-Book, Verso, London, 464 pp., 2002.

DeLong, K. L., Quinn, T. M., Taylor, F. W., Shen, C.-C., and Lin, K.: Improving coral-base paleoclimate reconstructions by replicating 350years of coral Sr/Ca variations, Palaeogeography, Palaeoclimatology, Palaeoecology, 373, 6–24, doi:10.1016/j.palaeo.2012.08.019, 2013.

Domínguez-Villar, D., Baker, A., Fairchild, I. J., and Edwards, R. L.: A method to anchor floating chronologies in annually laminated speleothems with U–Th dates, Quaternary Geochronology, 14, 57–66, doi:10.1016/j.quageo.2012.04.019, 2012.

Enmar, R., Stein, M., Bar-Matthews, M., Sass, E., Katz, A., and Lazar, B.: Diagenesis in live corals from the Gulf of Aqaba. I. The effect on paleo-oceanography tracers, Geochimica et Cosmochimica Acta, 64, 3123–3132, doi:10.1016/S0016-7037(00)00417-8, 2000.

Fischer, A. S., Terray, P., Guilyardi, E., Gualdi, S., and Delecluse, P.: Two Independent Triggers for the Indian Ocean Dipole/Zonal Mode in a Coupled GCM, J. Climate, 18, 3428–3449, doi:10.1175/JCLI3478.1, 2005.

Geen, R., Bordoni, S., Battisti, D. S., and Hui, K.: Monsoons, ITCZs, and the Concept of the Global Monsoon, Reviews of Geophysics, 58, doi:10.1029/2020RG000700, 2020.

Gopika, S., Izumo, T., Vialard, J., Lengaigne, M., Suresh, I., and Kumar, M. R. R.: Aliasing of the Indian Ocean externally-forced warming spatial pattern by internal climate variability, Clim Dyn, 54, 1093–1111, doi:10.1007/s00382-019-05049-9, 2020.

Hammer, O., Harper, D.A.T., and Ryan, P.D.: PAST: Paleontological Statistics Software Package for Education and Data Analysis: http://palaeo-electronica.org/2001_1/past/issue1_01.htm.

Hathorne, E. C., Gagnon, A., Felis, T., Adkins, J., Asami, R., Boer, W., Caillon, N., Case, D., Cobb, K. M., Douville, E., deMenocal, P., Eisenhauer, A., Garbe-Schönberg, D., Geibert, W., Goldstein, S., Hughen, K., Inoue, M., Kawahata, H., Kölling, M., Cornec, F. L., Linsley, B. K., McGregor, H. V., Montagna, P., Nurhati, I. S., Quinn, T. M., Raddatz, J., Rebaubier, H., Robinson, L., Sadekov, A., Sherrell, R., Sinclair, D., Tudhope, A. W., Wei, G., Wong, H., Wu, H. C., and You, C.-F.: Interlaboratory study for coral Sr/Ca and other element/Ca ratio measurements, Geochem. Geophys. Geosyst., 14, 3730–3750, doi:10.1002/ggge.20230, 2013.

860   Hendy, E. J., Gagan, M. K., Lough, J. M., McCulloch, M., and deMenocal, P. B.: Impact of skeletal dissolution and secondary aragonite on trace element and isotopic climate proxies in Porites corals, Paleoceanography, 22, doi:10.1029/2007PA001462, 2007.

Hiess, J., Condon, D. J., McLean, N., and Noble, S. R.: 238U/235U Systematics in terrestrial uranium-bearing minerals, Science, 335, 1610–1614, doi:10.1126/science.1215507, 2012.

865   Huang, B., Liu, C., Banzon, V., Freeman, E., Graham, G., Hankins, B., Smith, T., and Zhang, H.-M.: Improvements of the Daily Optimum Interpolation Sea Surface Temperature (DOISST) Version 2.1, Journal of Climate, 34, 2923–2939, doi:10.1175/JCLI-D-20-0166.1, 2021.

Jiang, J., Liu, Y., Mao, J., Li, J., Zhao, S., and Yu, Y.: Three Types of Positive Indian Ocean Dipoles and Their Relationships with the South Asian Summer Monsoon, Journal of Climate, 35, 405–424, doi:10.1175/JCLI-D-21-

870   0089.1, 2022.

Kalnay, E., Kanamitsu, M., Kistler, R., Collins, W., Deaven, D., Gandin, L., Iredell, M., Saha, S., White, G., Woollen, J., Zhu, Y., Leetmaa, A., Reynolds, R., Chelliah, M., Ebisuzaki, W., Higgins, W., Janowiak, J., Mo, K. C., Ropelewski, C., Wang, J., Jenne, R., and Joseph, D.: The NCEP/NCAR 40-Year Reanalysis Project, Bulletin of the American Meteorological Society, 77, 437–471, doi:10.1175/1520-0477(1996)077<0437:TNYRP>2.0.CO;2, 1996.

875   Lenssen, N. J. L., Schmidt, G. A., Hansen, J. E., Menne, M. J., Persin, A., Ruedy, R., and Zyss, D.: Improvements in the GISTEMP Uncertainty Model, Geophys Res Atmos, 124, 6307–6326, doi:10.1029/2018JD029522, 2019.

Leupold, M., Pfeiffer, M., Garbe-Schönberg, D., and Sheppard, C.: Reef-Scale-Dependent Response of Massive Porites Corals From the Central Indian Ocean to Prolonged Thermal Stress: Evidence From Coral Sr/Ca Measurements, Geochem. Geophys. Geosyst., 20, 1468–1484, doi:10.1029/2018gc007796, 2019.

880   Leupold, M., Pfeiffer, M., Watanabe, T. K., Reuning, L., Garbe-Schönberg, D., Shen, C.-C., and Brummer, G.-J. A.: El Niño–Southern Oscillation and internal sea surface temperature variability in the tropical Indian Ocean since 1675, Clim. Past, 17, 151–170, doi:10.5194/cp-17-151-2021, 2021.

Linsley, B. K., Wellington, G. M., and Schrag, D. P.: Decadal sea surface temperature variability in the subtropical South Pacific from 1726 to 1997 A.D, Science (New York, N.Y.), 290, 1145–1148, doi:10.1126/science.290.5494.1145, 2000.

885   McGregor, H. V. and Abram, N. J.: Images of diagenetic textures in Porites corals from Papua New Guinea and Indonesia, Geochem. Geophys. Geosyst., 9, doi:10.1029/2008GC002093, 2008.

Morice, C. P., Kennedy, J. J., Rayner, N. A., Winn, J. P., Hogan, E., Killick, R. E., Dunn, R. J. H., Osborn, T. J., Jones, P. D., and Simpson, I. R.: An Updated Assessment of Near-Surface Temperature Change From 1850: The HadCRUT5 Data Set, Geophys Res Atmos, 126, doi:10.1029/2019JD032361, 2021.

890   Murphy, R. J., Webster, J. M., Nothdurft, L., Dechnik, B., McGregor, H. V., Patterson, M. A., Sanborn, K. L., Webb, G. E., Kearney, L. I., Rintoul, L., and Erler, D. V.: High-resolution hyperspectral imaging of diagenesis and clays in fossil coral reef material: a nondestructive tool for improving environmental and climate reconstructions, Geochem. Geophys. Geosyst., 18, 3209–3230, doi:10.1002/2017GC006949, 2017.

Newcomb, K. R. and McCann, W. R.: Seismic history and seismotectonics of the Sunda Arc, J. Geophys. Res., 92, 421–439, 895   doi:10.1029/JB092iB01p00421, 1987.

Ng, B., Cai, W., Walsh, K., and Santoso, A.: Nonlinear processes reinforce extreme Indian Ocean Dipole events, Scientific reports, 5, 11697, doi:10.1038/srep11697, 2015.

PAST: Paleontological Statistics Software Package for Education and Data Analysis: http://palaeo-electronica.org/2001_1/past/issue1_01.htm.

900   Pfeiffer, M. and Dullo, W.-C.: Monsoon-induced cooling of the western equatorial Indian Ocean as recorded in coral oxygen isotope records from the Seychelles covering the period of 1840–1994AD, Quaternary Science Reviews, 25, 993–1009, doi:10.1016/j.quascirev.2005.11.005, 2006.

38

Pfeiffer, M., Watanabe, T. K., Takayanagi, H., Cahyarini, S. Y., Garbe-Schönberg, D., and Watanabe, T.: Coral Sr/Ca records provide realistic representation of eastern Indian Ocean cooling during extreme positive Indian Ocean Dipole events, Scientific reports, 12, 10642, doi:10.1038/s41598-022-14617-9, 2022.

Pfeiffer, M., Zinke, J., Dullo, W.-C., Garbe-Schönberg, D., Latif, M., and Weber, M. E.: Indian Ocean corals reveal crucial role of World War II bias for twentieth century warming estimates, Scientific reports, 7, 14434, doi:10.1038/s41598-017-14352-6, 2017.

Quinn, T. M. and Taylor, F. W.: SST artifacts in coral proxy records produced by early marine diagenesis in a modern coral from Rabaul, Papua New Guinea, Geophysical Research Letters, 33, doi:10.1029/2005GL024972, 2006.

R core team: R: A language and environment for statistical computing., 2023.

Reynolds, R. W., Rayner, N. A., Smith, T. M., Stokes, D. C., and Wang, W.: An Improved In Situ and Satellite SST Analysis for Climate, J. Climate, 15, 1609–1625, doi:10.1175/1520-0442(2002)015%3C1609:AIISAS%3E2.0.CO;2, 2002.

Ross, C. L., DeCarlo, T. M., and McCulloch, M. T.: Calibration of Sr/Ca, Li/Mg and Sr-U Paleothermometry in Branching and Foliose Corals, Paleoceanography and Paleoclimatology, 34, 1271–1291, doi:10.1029/2018pa003426, 2019.

Roxy, M. K., Ritika, K., Terray, P., and Masson, S.: The Curious Case of Indian Ocean Warming*,+, Journal of Climate, 27, 8501–8509, doi:10.1175/JCLI-D-14-00471.1, 2014.

Saji, N. H., Goswami, B. N., Vinayachandran, P. N., and Yamagata, T.: A dipole mode in the tropical Indian Ocean, Nature, 401, 360–363, doi:10.1038/43854, 1999.

Saji, N. H. and Yamagata, T.: Possible impacts of Indian Ocean Dipole mode events on global climate, Clim. Res., 25, 151–169, doi:10.3354/cr025151, 2003.

Sanchez, S. C., Westphal, N., Haug, G. H., Cheng, H., Edwards, R. L., Schneider, T., Cobb, K. M., and Charles, C. D.: A Continuous Record of Central Tropical Pacific Climate Since the Midnineteenth Century Reconstructed From Fanning and Palmyra Island Corals: A Case Study in Coral Data Reanalysis, Paleoceanography and Paleoclimatology, 35, doi:10.1029/2020PA003848, 2020.

Sayani, H. R., Cobb, K. M., Cohen, A. L., Elliott, W. C., Nurhati, I. S., Dunbar, R. B., Rose, K. A., and Zaunbrecher, L. K.: Effects of diagenesis on paleoclimate reconstructions from modern and young fossil corals, Geochimica et Cosmochimica Acta, 75, 6361–6373, doi:10.1016/j.gca.2011.08.026, 2011.

Sayani, H. R., Cobb, K. M., Monteleone, B., and Bridges, H.: Accuracy and Reproducibility of Coral Sr/Ca SIMS Timeseries in Modern and Fossil Corals, Geochem. Geophys. Geosyst., 23, doi:10.1029/2021GC010068, 2022.

Schott, F. A., Xie, S.-P., and McCreary, J. P.: Indian Ocean circulation and climate variability, Reviews of Geophysics, 47, doi:10.1029/2007RG000245, 2009.

Schrag, D. P.: Rapid analysis of high-precision Sr/Ca ratios in corals and other marine carbonates, Paleoceanography, 14, 97–102, doi:10.1029/1998PA900025, 1999.

Schreck, C., Lee, H.-T., and Knapp, K.: HIRS Outgoing Longwave Radiation—Daily Climate Data Record: Application toward Identifying Tropical Subseasonal Variability, Remote Sensing, 10, 1325, doi:10.3390/rs10091325, 2018.

Shen, C.-C., Wu, C.-C., Cheng, H., Lawrence Edwards, R., Hsieh, Y.-T., Gallet, S., Chang, C.-C., Li, T.-Y., Lam, D. D., Kano, A., Hori, M., and Spötl, C.: High-precision and high-resolution carbonate 230Th dating by MC-ICP-MS with SEM protocols, Geochimica et Cosmochimica Acta, 99, 71–86, doi:10.1016/j.gca.2012.09.018, 2012.

Smodej, J., Reuning, L., Wollenberg, U., Zinke, J., Pfeiffer, M., and Kukla, P. A.: Two-dimensional X-ray diffraction as a tool for the rapid, nondestructive detection of low calcite quantities in aragonitic corals, Geochem. Geophys. Geosyst., 16, 3778–3788, doi:10.1002/2015GC006009, 2015.

39

Steinke, S., Mohtadi, M., Prange, M., Varma, V., Pittauerova, D., and Fischer, H. W.: Mid- to Late-Holocene Australian–
945   Indonesian summer monsoon variability, Quaternary Science Reviews, 93, 142–154,
doi:10.1016/j.quascirev.2014.04.006, 2014a.

Steinke, S., Prange, M., Feist, C., Groeneveld, J., and Mohtadi, M.: Upwelling variability off southern Indonesia over the
past two millennia, Geophysical Research Letters, 41, 7684–7693, doi:10.1002/2014GL061450, 2014b.

Susanto, R. D., Gordon, A. L., and Zheng, Q.: Upwelling along the coasts of Java and Sumatra and its relation to ENSO,
950   Geophys. Res. Lett., 28, 1599–1602, doi:10.1029/2000GL011844, 2001.

Toms, J. D. and Lesperance, M. L.: Piecewise regression: a tool for identifying ecological thresholdsPIECEWISE
REGRESSION: A TOOL FOR IDENTIFYING ECOLOGICAL THRESHOLDS, Ecology, 84, 2034–2041,
doi:10.1890/02-0472, 2003.

Torrence, C. and Compo, G. P.: A Practical Guide to Wavelet Analysis, Bulletin of the American Meteorological Society,
955   79, 61–78, doi:10.1175/1520-0477(1998)079<0061:APGTWA>2.0.CO;2, 1998.

Ummenhofer, C. C., England, M. H., McIntosh, P. C., Meyers, G. A., Pook, M. J., Risbey, J. S., Gupta, A. S., and Taschetto,
A. S.: What causes southeast Australia's worst droughts?, Geophys. Res. Lett., 36, doi:10.1029/2008GL036801, 2009a.

Ummenhofer, C. C., Sen Gupta, A., England, M. H., and Reason, C. J. C.: Contributions of Indian Ocean Sea Surface
Temperatures to Enhanced East African Rainfall, J. Climate, 22, 993–1013, doi:10.1175/2008JCLI2493.1, 2009b.

960 Villiers, S. de, Greaves, M., and Elderfield, H.: An intensity ratio calibration method for the accurate determination of
Mg/Ca and Sr/Ca of marine carbonates by ICP-AES, Geochem. Geophys. Geosyst., 3, doi:10.1029/2001GC000169,
2002.

Villiers, S. de, Shen, G. T., and Nelson, B. K.: The -temperature relationship in coralline aragonite: Influence of variability
in and skeletal growth parameters, Geochimica et Cosmochimica Acta, 58, 197–208, doi:10.1016/0016-7037(94)90457-
965   x, 1994.

Watanabe, T. K. and Pfeiffer, M.: A Simple Monte Carlo Approach to Estimate the Uncertainties of SST and δ 18 O sw
Inferred From Coral Proxies, Geochem. Geophys. Geosyst., 23, doi:10.1029/2021GC009813, 2022.

Webster, P. J., Moore, A. M., Loschnigg, J. P., and Leben, R. R.: Coupled ocean-atmosphere dynamics in the Indian Ocean
during 1997-98, Nature, 401, 356–360, doi:10.1038/43848, 1999.

970 Weller, E. and Cai, W.: Meridional variability of atmospheric convection associated with the Indian Ocean Dipole Mode,
Scientific reports, 4, 3590, doi:10.1038/srep03590, 2014.

Weller, E., Cai, W., Min, S.-K., Wu, L., Ashok, K., and Yamagata, T.: More-frequent extreme northward shifts of eastern
Indian Ocean tropical convergence under greenhouse warming, Scientific reports, 4, 6087, doi:10.1038/srep06087, 2014.

Yang, K., Cai, W., Huang, G., Wang, G., Ng, B., and Li, S.: Oceanic Processes in Ocean Temperature Products Key to a
975   Realistic Presentation of Positive Indian Ocean Dipole Nonlinearity, Geophys. Res. Lett., 47,
doi:10.1029/2020GL089396, 2020.

Zhang, H.: Diagnosing Australia-Asian monsoon onset/retreat using large-scale wind and moisture indices, Clim Dyn, 35,
601–618, doi:10.1007/s00382-009-0620-x, 2010.

Zinke, J., Dullo, W.-C., Heiss, G. A., and Eisenhauer, A.: ENSO and Indian Ocean subtropical dipole variability is recorded
980   in a coral record off southwest Madagascar for the period 1659 to 1995, Earth and Planetary Science Letters, 228, 177–
194, doi:10.1016/j.epsl.2004.09.028, 2004.

Zinke, J., Reuning, L., Pfeiffer, M., Wassenburg, J. A., Hardman, E., Jhangeer-Khan, R., Davies, G. R., Ng, C. K. C., and
Kroon, D.: A sea surface temperature reconstruction for the southern Indian Ocean trade wind belt from corals in
Rodrigues Island (19° S, 63° E), Biogeosciences, 13, 5827–5847, doi:10.5194/bg-13-5827-2016, 2016.

40

985   Zinke, J., Watanabe, T. K., Rühs, S., Pfeiffer, M., Grab, S., Garbe-Schönberg, D., and Biastoch, A.: A 334-year coral record
         of surface temperature and salinity variability in the greater Agulhas Current region, Clim. Past, 18, 1453–1474,
         doi:10.5194/cp-18-1453-2022, 2022.